

Research Programme of the Research Fund for Coal and Steel - Steel RTD

*Project carried out with a financial grant of the
Research Programme of the Research Fund for Coal and Steel*

HOLLOSSTAB

Overall-Slenderness Based Direct Design for Strength and Stability of Innovative Hollow Sections

Grant Agreement Number: RFCS-2015-709892

Deliverable D9.1 - Dissemination

Design Guidelines for INNOVATIVE BUCKLING DESIGN RULES FOR STRUCTURAL HOLLOW SECTIONS

1st Edition, June 2019

Authors:

Andreas Taras	(Bundeswehr University Munich)
Andrea Toffolon	(“)
Igor Niko	(“)
Leroy Gardner	(Imperial College London)
Xin Meng	(“)
Dinar Camotim	(Técnico Lisboa)
Rodrigo Gonçalves	(Universidade NOVA de Lisboa)
Alain Bureau	(Centre Technique Industriel de la Construction Métallique)
André Beyer	(“)
Gorka Iglesias Toquero	(ArcelorMittal, formerly CONDESA)
Véronique Dehan	(European Convention for Constructional Steelwork)

PREFACE

These Design Guidelines represent the deliverable D9.1 of the RFCS-funded research project *HOLLOSSTAB* (RFCS Grant Agreement Nr. 2015-709892), which was conducted at the authors' research institutes and organizations between July 2016 and June 2019. The project led to the development of new design rules for the verification of the cross-sectional and member stability and strength of hollow sections of various shapes and steel grades. The new design rules are applications of the Generalised Slenderness-based Resistance Method (GSRM), which was formulated during the *HOLLOSSTAB* project as an extension and improvement of existing concepts for the stability design of steel sections and members.

These Design Guidelines contain an overview of the research work carried out during the project, give a concise summary of the developed GSRM design rules for the design of hollow sections, and provide an extensive set of worked examples, which serve to facilitate the understanding of the GSRM design methods and of their practical implementation. The intended readership of these Design Guidelines thus includes researchers aiming to obtain an overview of the *HOLLOSSTAB* project through a more compact document than the full scientific project reports, as well as practitioners desiring to apply in practice the new GSRM design rules.

CONTENTS

<i>Preface</i>	<i>III</i>
1 INTRODUCTION - MOTIVATION AND SCOPE	7
1.1 MOTIVATION FOR THE PROJECT "HOLLOSSTAB"	7
1.2 CONTENT OF THESE GUIDELINES	10
2 Overview of Current EC3 Design Rules	11
2.1 DESIGN CHECKS FOR CROSS-SECTIONAL CAPACITY	11
2.2 DESIGN CHECKS FOR MEMBER STABILITY	14
3 Summary of Developments in "HOLLOSSTAB"	17
3.1 GENERAL METHODOLOGY	17
3.2 PHYSICAL TESTS, FEM-MODEL CALIBRATION, PARAMETRIC STUDY	17
3.2.1 <i>Rectangular and Square Hollow Sections (RHS/SHS)</i>	17
3.2.2 <i>Cylindrical and Elliptical Hollow Sections (CHS/EHS)</i>	23
3.3 DEVELOPMENT AND CALIBRATION OF DESIGN RULES.....	26
3.4 SOFTWARE TOOL.....	35
4 Design Recommendation	37
4.1 RECOMMENDATIONS FOR CROSS-SECTIONAL CAPACITY CHECKS	37
4.1.1 <i>Common definitions</i>	37
4.1.2 <i>GSRM rules for RHS/SHS</i>	37
4.1.3 <i>GSRM rules for CHS/EHS</i>	38
4.1.4 <i>Alternative rules for CHS/EHS in the plastic range - CSM/GSRM approach</i>	39
4.1.5 <i>Alternative rules for RHS/SHS in the plastic range - CSM/GSRM approach</i>	41
4.2 RECOMMENDATIONS FOR MEMBER BUCKLING CHECKS.....	42
4.2.1 <i>Common definitions</i>	42
4.2.2 <i>GSRM rules for RHS/SHS and CHS/EHS (Approach 2)</i>	42
4.2.3 <i>GSRM rules for CHS/EHS (Approach 1)</i>	42
5 WORKED EXAMPLES	46
5.1 EXAMPLE 1 - CROSS-SECTIONAL CAPACITY, RHS 250X150X5, EN10219, S700.....	47
5.1.1 <i>Design according to EC3</i>	47
5.1.2 <i>HOLLOSSTAB design method</i>	50
5.1.3 <i>Summary of results</i>	51
5.2 EXAMPLE 2 - CROSS-SECTIONAL CAPACITY, RHS 180X120X8, EN10210, S460.....	52
5.2.1 <i>Design according to EC3</i>	53
5.2.2 <i>HOLLOSSTAB design method</i>	55
5.2.3 <i>Summary of results</i>	56
5.3 EXAMPLE 3 - CROSS-SECTIONAL CAPACITY, RHS 200X100X6.3, EN10219, S460.....	57
5.3.1 <i>Design according to EC3</i>	58
5.3.2 <i>HOLLOSSTAB design method</i>	59
5.3.3 <i>Summary of results</i>	60
5.4 EXAMPLE 4 - CROSS-SECTIONAL CAPACITY, EHS200X100X10, EN10210-2, S355.....	61
5.4.1 <i>Design according to EC3</i>	61
5.4.2 <i>HOLLOSSTAB design method (deformation-based approach)</i>	63

5.4.3	<i>Summary of results</i>	64
5.5	EXAMPLE 5 - MEMBER BUCKLING, SHS200x200x6.3, EN10210, S690.....	65
5.5.1	<i>Design according to EC3</i>	65
5.5.2	<i>HOLLOSSTAB design method</i>	68
5.5.3	<i>Summary of results</i>	70
5.6	EXAMPLE 6 - MEMBER BUCKLING, CHS60.3x3, EN10219-2, S700.....	71
5.6.1	<i>Design according to EC3</i>	71
5.6.2	<i>HOLLOSSTAB design method</i>	73
5.6.3	<i>Summary of results</i>	74
	<i>References</i>	75

1 INTRODUCTION - MOTIVATION AND SCOPE

1.1 Motivation for the Project "HOLLOSSTAB"

Recent construction practice has seen a rise in the use of structural hollow sections, due to the appealing aesthetics as well as better awareness of the advantages in terms of strength and stiffness of this type of section. In order to meet the increasing demands for sustainable and economic construction typologies and methods, the European steel industry, and particularly the producers of structural hollow sections, are aiming for a reduction of weight and emissions through the use of more thin-walled sections and/or higher-strength steel grades (with yield strength $f_y \geq 460$ MPa). These innovations increase the economy and sustainability of construction projects through the reduction of weld volumes, erection times and foundation costs. Especially the introduction of higher-strength steel grades into standard construction practice is a relevant industrial goal for the European steel industry, offering chances for new product development, research and innovation, and thus market advantages.

However, the introduction of more slender construction typologies for hollow sections leads to a number of scientific and engineering challenges: higher material strength ($R_e/R_{p0.2}$ or f_y ; R_m or f_u), with different constitutive laws (shorter or inexistent plastic plateau, diminished ultimate strain) combined with thinner plates leads to an increased significance of instability phenomena, especially of local buckling phenomena and their interaction with the “global” instability mode of flexural buckling.

Preliminary studies have shown that the application of current design codes (e.g. the Eurocodes) is either ineffective, uneconomical or – in some cases - altogether impossible for combined instability phenomena in slender, high-strength hollow sections:

1. At the level of cross-sectional resistances, by its definition an increase of yield strength f_y leads to an increase of the (local, “L”) normalized slenderness $\bar{\lambda} = \sqrt{f_y/\sigma_{cr}}$. This means that more sections will fall into the non-compact (class 3) or slender (class 4) range and are thus more sensitive to local buckling phenomena. The current classification system is quite often not suitable for capturing the actual cross-sectional behaviour in terms of strength:
 - i. it predicts a sudden – and not realistic – decrease of strength at the class 2 to 3 transition,
 - ii. the classification is based on c/t limits and in turn on bifurcation stresses for individual plates, omitting all mutual supporting effects of adjacent components,

INTRODUCTION

- **iii.** plasticity is completely omitted in the non-compact and slender range, while strain hardening is omitted in the compact range,
- **iv.** the strength for class 4 sections is usually calculated by separating the load components (axial force and bending moments) and determining “effective cross-sections” for these individual load cases, creating an artificial separation of the real stress state, and
- **v.** for circular (CHS) and elliptical (EHS) hollow sections, point iv is altogether inapplicable, as no definition of effective areas for cylindrical sections is given in current design codes such as Eurocode 3, EN 1993-1-1 [1]; reference to the shell buckling code EN 1993-1-6 is made instead, which is largely inapplicable and inconsistent with applications for cylindrical hollow section members. Only the latest draft version of the planned re-edition of EN 1993-1-1, prEN1993-1-1:2018 [2] introduced some (conservative) definitions of effective cross-sections for cylindrical sections.

Point **i.** was already partly addressed (for mild steel sections) in the RFCS project “SEMI-COMP”, see Figure 1a. However, points **ii.** to **v.** were not addressed in that project, making an immediate code implementation easier, but rendering them less suitable for innovative applications. This is further illustrated in Figure 1b, where experimental results of axial compression and bending strength are plotted over the plate/shell slenderness: the “over-strength”, when compared to code predictions, is particularly visible for the CHS in bending (effect of mutual support of cross-sectional parts) and generally for low slenderness (strain hardening).

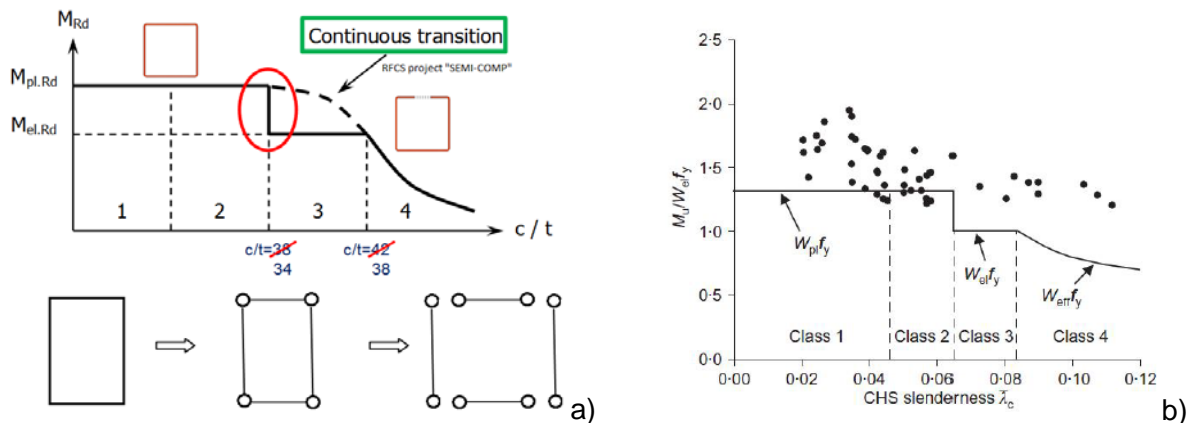


Figure 1: Conventional classification system for strength, based on 4 cross-sectional classes; discontinuity at the class 2-3 border, solution proposed in RFCS “SEMI-COMP” project, classification based on individual plates (a); Experimental results: cross-section resistance as a function of plate slenderness; stub-columns, CHS in bending (b)

2. Beyond the cross-sectional level, instability phenomena become more prevalent also at a global (“G”) level (flexural buckling) when interacting with the local (“L”) resistance, leading to an “L+G” instability phenomena. These effects are treated

in structural design codes in a manner that is potentially too conservative for the high-strength, slender hollow sections studied in this project.

3. The peculiarities of high-strength materials (σ - ε curves) and sections (lower residual stresses levels relative to strength, different imperfection levels) are only superficially studied and addressed in design codes.
4. Generally, the treatment of local, global, and interactive L+G instabilities in the Eurocode and other international design codes is seen as too cumbersome by many designers and does not take full advantage of already-available numerical computational methods.

Combined, these drawbacks represent a hindrance to the further development and market introduction of more slender hollow section members in Europe. In order to overcome them, innovative design methods must be introduced and the corresponding scientific background and knowledge must be gathered. Thereby, the new rules should be combined with bespoke, free-ware software tools in order to make the new method simple to use and practical for engineers in design offices and steel construction companies. The development of these rules and software tools was the objective of the RFCS Project HOLLOSSTAB.

Thereby, the development of a specific type of design rule was envisaged in HOLLOSSTAB, termed the **G**eneralised **S**lenderness-based **R**esistance **M**ethod (GSRM). This method, similarly to other recently proposed methods such as the General Method for the design of whole frames ([3], [4]), the Direct Strength Method (DSM, [5], [6], [7]), the Continuous Strength Method (CSM, [8], [9]) and – in the most directly related way - the Overall Interaction Concept / Overall Method (OIC, [9], [11]) makes use of an “overall” definition of the cross-sectional and member slenderness, generalised to account for combined load cases and the mutual support provided by the various parts of the studied cross-section and member. This requires the development of the mentioned, bespoke software tools for a straightforward use.

The generalised definitions of slenderness and resistance make use of load amplification factors to reach a certain defined condition or resistance, and thus termed “R”.

Thereby, the generalised slenderness is defined as $\bar{\lambda} = \sqrt{R_{ref}/R_{cr}}$

while the ultimate (buckling) resistance is defined as $R_b = \chi \cdot R_{ref}$

with the buckling coefficient χ being a function of $\bar{\lambda}$.

Figure 2 shows the general procedure of the GSRM design approach, shown for the case of local buckling respectively cross-sectional strength, with index “L”. It needs to be stressed that the definition of the various functions for χ is the *main challenge of this type of approach and was thus one of the main results of HOLLOSSTAB’s developments.*

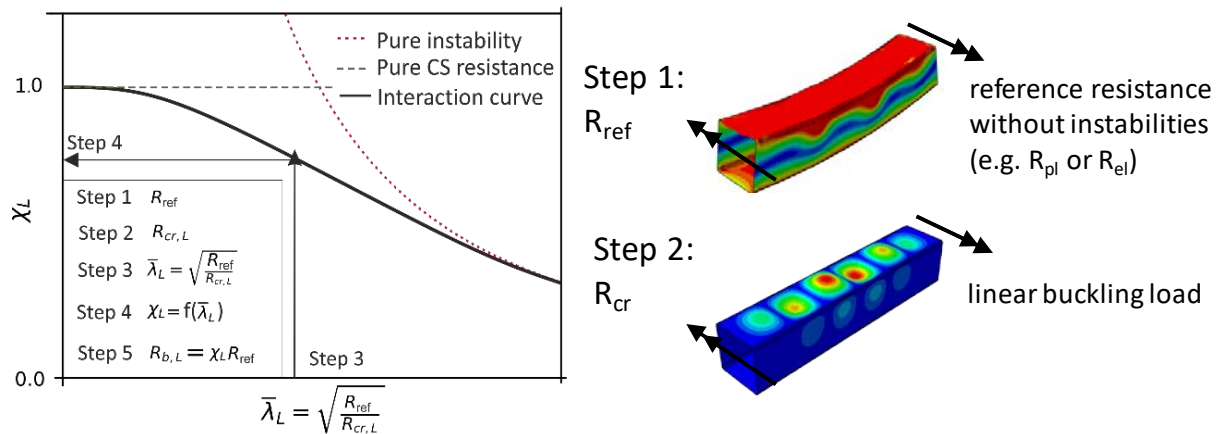


Figure 2: Steps of HOLLOSSTAB's Generalised Slenderness-based Resistance Method – GSRM – application to the cross-sectional resistance (local buckling, index “L”).

1.2 Content of these Guidelines

These Design Guidelines represent one of the deliverables of the RFCS research project HOLLOSSTAB. They contain a succinct review of the project's aims and research work, an overview of the developed design rules and their justification and a series of worked examples to clarify the proposed new design methodologies.

The document is structured as follows:

- Following this introductory chapter, a short overview of current design rules for hollow sections in Eurocode 3 is given in Chapter 2, based on the latest version of prEN1993-1-1:2018 [2].
- In Chapter 3, the research work carried out during the RFCS project HOLLOSSTAB is briefly summarized. Thereby, the physical and numerical tests carried out for the project are illustrated the main aspects of the developed design rules are shown and justified. Finally, the developed design software is presented.
- In Chapter 4, the proposed, GSRM-type design rules are summarized.
- Extensive worked examples are finally presented in Chapter 5

2 OVERVIEW OF CURRENT EC3 DESIGN RULES

A short overview of current design rules for hollow sections in Eurocode 3 is given in this chapter. This overview is thereby based on the most recently distributed version of the pre-standard prEN1993-1-1:2018 [2], which is set to replace the 2005 version of EN1993-1-1 [1] valid to date. This standard contains some amendments to the current code that are of relevance to the design of hollow sections, such as some changes to the cross-sectional classification, the design of cylindrical and elliptical sections, and the design of semi-compact (class 3) sections. This review is given in order to clarify what design rules are being referred to in this guideline when referencing Eurocode 3 and comparing it to the new GSRM rules.

2.1 Design Checks for Cross-Sectional Capacity

In Eurocode 3 (prEN 1993-1-1:2018 and all previous versions), the choice of methods and formulae for the evaluation of the cross-sectional resistance (and subsequently of the member resistance) is based on the initial step of the classification of the cross-section into one of four different cross-sectional classes. These are defined by the difference proneness to (local) plate buckling phenomena in the constitutive cross-section walls subjected to compression. The specific level of resistance (plastic, elastic or even lower-than-elastic) varies according to the four classes. This is schematically shown for a double symmetric I-section loaded in strong-axis bending in Figure 3.

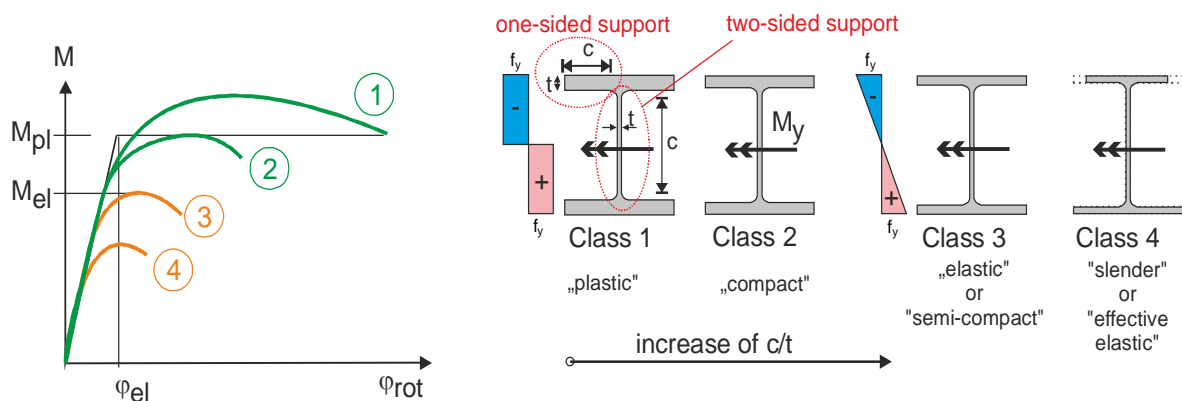


Figure 3: Rotation capacity and classification of cross-sections into four classes.

The classification of a cross-section is carried out by considering the width-to-thickness ratios of the individual cross-section walls (plates) in compression, to the stress gradient in these plates and to the support conditions (internal and outstand) of each wall.

Compared to the 2006 version of EN1993-1-1, the current draft version prEN1993-1-1:2018 contains a number of changes to the cross-sectional classification methods and limits that particularly affect hollow sections. For this reason, the pertinent tables are shown below, see Table 1 and Table 2.

Table 1: Classification of cross-sections based on internal walls in prEN1993-1-1:2018; this covers rectangular and square hollow sections (RHS and SHS)

Internal compression parts			
		$c = h - 3t$	
		$c = b - 3t$	
Key: 1: Axis of bending			
Stress distribution in parts (compression positive)			
Class 1	$c/t \leq 72 \epsilon$	$c/t \leq 28 \epsilon$	when $\alpha_c > 0,5$: $c/t \leq \frac{126 \epsilon}{5,5 \alpha_c - 1}$ when $\alpha_c \leq 0,5$: $c/t \leq \frac{36 \epsilon}{\alpha_c}$
Class 2	$c/t \leq 83 \epsilon$	$c/t \leq 34 \epsilon$	when $\alpha_c > 0,5$: $c/t \leq \frac{188 \epsilon}{6,53 \alpha_c - 1}$ when $\alpha_c \leq 0,5$: $c/t \leq \frac{41,5 \epsilon}{\alpha_c}$
Stress distribution in parts (compression positive)			
Class 3	$c/t \leq 121 \epsilon$	$c/t \leq 38 \epsilon$	when $\psi > -1$: $c/t \leq \frac{38 \epsilon}{0,608 + 0,343 \psi + 0,049 \psi^2}$ when $\psi \leq -1^*$: $\frac{c}{t} \leq 60,5 \epsilon (1 - \psi)$
*) $\psi \leq -1$ and a compression stress of $\sigma_{com,Ed} = f_y$ applies where the tensile strain $\epsilon_t > f_y/E$			

Table 2: Classification of cross-sections with cylindrical walls in prEN1993-1-1:2018; this covers circular and elliptical hollow sections (CHS and EHS)

Circular and elliptical hollow sections			
	Section in compression	Section in bending	Compression and bending
Class 1	$d_e/t \leq 50 \varepsilon^2$	$d_e/t \leq 50 \varepsilon^2$	$d_e/t \leq 50 \varepsilon^2$
Class 2	$d_e/t \leq 70 \varepsilon^2$	$d_e/t \leq 70 \varepsilon^2$	$d_e/t \leq 70 \varepsilon^2$
Class 3	$d_e/t \leq 90 \varepsilon^2$	$d_e/t \leq 140 \varepsilon^2$	$d_e/t \leq \frac{2520 \varepsilon^2}{5\psi + 23}$
Equivalent diameter d_e for circular and elliptical hollow sections			
For circular hollow sections:	$d_e = d$		
For elliptical hollow sections:	<p>In compression: $d_e = h \left[1 + \left(1 - 2,3 \left(\frac{t}{h} \right)^{0,6} \right) \left(\frac{h}{b} - 1 \right) \right]$ or, conservatively: $d_e = \frac{h^2}{b}$</p> <p>In bending about the strong axis: For $h/b \leq 1,36$: $d_e = \frac{b^2}{h}$ For $h/b > 1,36$: $d_e = 0,4 \frac{h^2}{b}$</p> <p>In bending about the weak axis, or compression and bending about the weak axis: $d_e = \frac{h^2}{b}$</p> <p>In compression and bending about the strong axis, the equivalent diameter d_e may be determined by linear interpolation between the equivalent diameter for compression and that for bending based on the parameter α_c for Class 1 and Class 2 cross-sections and ψ for Class 3 and Class 4 cross-sections.</p> <p>In compression and biaxial bending, the equivalent diameter d_e may be taken as the interpolated equivalent diameter for compression and bending about the strong axis, as described above, but with α_c and ψ determined using a modified axial force equal to $N_{Ed} + M_{z,Ed} A/W_{pl,z}$ for Class 1 and Class 2 cross-sections and $N_{Ed} + M_{z,Ed} A/W_{el,z}$ for Class 3 and Class 4 cross-sections.</p>		

The class of the cross-section is finally defined as the highest class of those of the individual walls. For class 1 and class 2 sections, the ideal-plastic resistance defined by the theoretical presence of the yield stress and notionally limitless strains may be used for design purposes. For class 4 (slender) cross-sections, local buckling occurs before the yielding is achieved in any fibre; the effective width method is used for

the design of these sections. Semi-compact, class 3 sections may be designed by either of the following two methods:

- either by limiting the cross-sectional resistance to the level of loading that leads to the first exceedance of the yield stress in any fibre.
- or by the elasto-plastic, transitional resistance given by the method now found in Annex B of prEN1993-1-1:2018 and originally developed in the RFCS project SEMI-COMP, see [12].

For reasons of brevity in the present Design Guidelines, these rules are not further illustrated here and the reader is referred to the cited draft standard and publications for further details. However, it shall be stated that the following procedures and design rules were adopted as the basis for all comparisons of the new GSRM design rules developed in HOLLOSSTAB, as well as of physical and numerical test results, with “Eurocode 3” design rules:

- the classification of the cross-sections was based on an amplification of the stress state given by the considered load case up to the limit needed for classification, which varies in dependence of the considered class. This means that all loads were amplified proportionally; other methods of classification may exist but are not well suited for a comparison with the GSRM design methods developed in HOLLOSSTAB.
- for sections that were classified into class 1 and class 2, the ideal-plastic resistance given in section 8.2 of prEN1993-1-1:2018 was used. This resistance may differ in some respects from a fully mechanically derived resistance based on equilibrium alone.
- for sections that were classified into class 3, the SEMI-COMP method was applied, see Annex B of prEN1993-1-1:2018.
- for class 4 sections, the effective width method was applied, whereby the calculation of the effective area A_{eff} and section moduli $W_{y,\text{eff}}$ and $W_{z,\text{eff}}$ was carried out for the individual load cases; this is an allowed and most commonly used methodology in (pr)EN1993-1-1.

2.2 Design Checks for Member Stability

The principal analytical method used in EN 1993-1-1 for the check of the resistance against global buckling (member buckling) is represented by two so-called interaction formulae, given in sections 6.3.3 respectively 8.3.3 of EN 1993-1-1 and prEN1993-1-1:2018. These cover the potential buckling modes about the yy-axis and the z-z-axis. They have been derived and validated for members with double-symmetrical cross-section and thus cover most types of hollow section.

- buckling dominated by bending about the y-y axis:

$$\frac{N_{Ed}}{\chi_y N_{Rk}} + k_{yy} \frac{M_{y,Ed} + \Delta M_{y,Ed}}{\chi_{LT} \frac{M_{y,Rk}}{\gamma_{M1}}} + k_{yz} \frac{M_{z,Ed} + \Delta M_{z,Ed}}{\frac{M_{z,Rk}}{\gamma_{M1}}} \leq 1,0$$

- buckling dominated by bending about the z-z and/or torsional deformations:

$$\frac{N_{Ed}}{\chi_z N_{Rk}} + k_{zy} \frac{M_{y,Ed} + \Delta M_{y,Ed}}{\chi_{LT} \frac{M_{y,Rk}}{\gamma_{M1}}} + k_{zz} \frac{M_{z,Ed} + \Delta M_{z,Ed}}{\frac{M_{z,Rk}}{\gamma_{M1}}} \leq 1,0$$

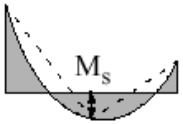
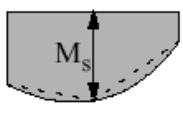
In the case of hollow sections of usual dimension, χ_{LT} may be set to 1,0 since lateral-torsional buckling is not relevant, and the interaction coefficients in Table 3 may be used. The definition and the values of each of the coefficients k_{yy} , k_{yz} , k_{zy} and k_{zz} are provided in prEN 1993–1–1 for Class 1, Class 2, Class 3 and Class 4 cross-sections. Thereby, for Class 3 sections either the pure elastic bending resistance $W_{el}f_y$ or the elasto-plastic bending resistance $W_{ep}f_y$ of the SEMI-COMP method (Annex B of prEN1993-1-1:2018, see [12]) may be used in combination with the corresponding values of the interaction coefficients.

Table 3: Interaction coefficients for member buckling checks of hollow sections in prEN1993-1-1:2018

Plastic cross-sectional properties Class 1, Class 2, Class 3 (with W_{ep} according to Annex B)	Elastic cross-sectional properties Class 3(with W_{el}), Class 4
For $\bar{\lambda}_y < 1,0$: $k_{yy} = C_{my}[1 + (\bar{\lambda}_y - 0,2) n_y]$	For $\bar{\lambda}_y < 1,0$: $k_{yy} = C_{my}(1 + 0,6 \bar{\lambda}_y n_y)$
For $\bar{\lambda}_y \geq 1,0$: $k_{yy} = C_{my}(1 + 0,8 n_y)$	For $\bar{\lambda}_y \geq 1,0$: $k_{yy} = C_{my}(1 + 0,6 n_y)$
$k_{yz} = 0,6 k_{zz}$	$k_{yz} = k_{zz}$,
$k_{zy} = 0,6 k_{yy}$	$k_{zy} = 0,8 k_{yy}$
For $\bar{\lambda}_z < 1,0$: $k_{zz} = C_{mz}[1 + (\bar{\lambda}_z - 0,2) n_z]$ For $\bar{\lambda}_z \geq 1,0$: $k_{zz} = C_{mz}[1 + 0,8 n_z]$	For $\bar{\lambda}_z < 1,0$: $k_{zz} = C_{mz}(1 + 0,6 \bar{\lambda}_z n_z)$ For $\bar{\lambda}_z \geq 1,0$: $k_{zz} = C_{mz}(1 + 0,6 n_z)$

The equivalent uniform moment factors C_m to be applied for isolated members with hinged boundary conditions at both ends are shown in Table 4.

Table 4: Equivalent uniform moment factors C_m for isolated members in prEN1993-1-1:2018

Moment diagram	Range		C_{my} and C_{mz} and C_{mLT}	
			Uniform loading	Concentrated load
	$-1 \leq \psi \leq 1$		$0,6 + 0,4\psi \geq 0,4$	
 $\alpha_s = M_s / M_h$	$0 \leq \alpha_s \leq 1$	$-1 \leq \psi \leq 1$	$0,2 + 0,8\alpha_s \geq 0,4$	$0,2 + 0,8\alpha_s \geq 0,4$
	$-1 \leq \alpha_s < 0$	$0 \leq \psi \leq 1$	$0,1 - 0,8\alpha_s \geq 0,4$	$-0,8\alpha_s \geq 0,4$
		$-1 \leq \psi < 0$	$0,1(1-\psi) - 0,8\alpha_s \geq 0,4$	$-0,2\psi - 0,8\alpha_s \geq 0,4$
 $\alpha_h = M_h / M_s$	$0 \leq \alpha_h \leq 1$	$-1 \leq \psi \leq 1$	$0,95 + 0,05\alpha_h$	$0,90 + 0,10\alpha_h$
	$-1 \leq \alpha_h < 0$	$0 \leq \psi \leq 1$	$0,95 + 0,05\alpha_h$	$0,90 + 0,10\alpha_h$
		$-1 \leq \psi < 0$	$0,95 + 0,05\alpha_h(1+2\psi)$	$0,90 + 0,10\alpha_h(1+2\psi)$

The resistance check of the member end sections must be carried out in addition to the member check and can become critical if the equivalent moment factors C_m are significantly smaller than 1,0 or if the member is very short.

In order to compare the results of the above rules of prEN1993-1-1:2018 with the design rules developed in *HOLLOSSTAB* and with physical and numerical tests, the interaction formulae of Eurocode 3 had to be evaluated by introducing a load amplification factor R_{EC3} as a multiplier for all relevant load components N_{Ed} , $M_{y,Ed}$ and $M_{z,Ed}$. R_{EC3} was increased until the equations yielded a utilization value of 1,0.

3 SUMMARY OF DEVELOPMENTS IN “HOLLOSSTAB”

In this chapter, the research work carried out during the RFCS project *HOLLOSSTAB* is briefly summarized. Thereby, the physical and numerical tests carried out for the project are illustrated the main aspects of the developed design rules are shown and justified. Finally, the developed design software is presented.

3.1 General Methodology

The development of new design rules – and design tools – during the RFCS project *HOLLOSSTAB* followed the following steps:

1. In an extensive physical test campaign, more than 150 full-scale specimens of short and long columns and beam-columns were tested in various combinations of compression and bending. Simultaneously, auxiliary tests and measurements were carried out to characterize the material, geometry and imperfections of the tested specimens.
2. Numerical, FEM shell-element models were developed and calibrated to closely reproduce the strength and deformation results obtained in the physical tests.
3. These validated and verified numerical models were used to carry out an extensive numerical parametric study, as a means to further enhance the studied parameter range and the knowledge obtained from the physical tests through “numerical tests”, thus expanding the total number of by two orders of magnitude.
4. Analytical, practical design formulae in the GSRM-format were developed for the local/cross-sectional (L), global/member (G) and G+L level, through a combination of mechanical derivations and model calibration to the comprehensive pool of physical and numerical tests.
5. The reliability of the design formulae were evaluated and the partial factors have been calculated.
6. A software tool was developed in order to efficiently carry out the design tasks needed for the new GSRM design of hollow sections.

Extensive background for these steps may be found in the [13] to [19]

3.2 Physical Tests, FEM-Model Calibration, Parametric Study

3.2.1 Rectangular and Square Hollow Sections (RHS/SHS)

HOLLOSSTAB's experimental programme on standard RHS and SHS sections made to [20] and [21], as well as additional, custom-made sections with stiffened flat

faces and/or polygonal cross-section, was conducted in the Structural Engineering Laboratories at Bundeswehr University Munich, Imperial College London and the University of Lisbon (Técnico Lisboa), and comprised more than 100 individual tests. Sections of steel grade S355 to S770 were considered and tested in compression or various combinations of compression and bending. The tests comprised shorter members, with the aim of studying the behaviour at the cross-sectional level, as well as longer members, needed to study the behaviour of beam-columns failing in global (G or G+L) buckling. Figure 4 gives an overview of the studied cross-section shapes.

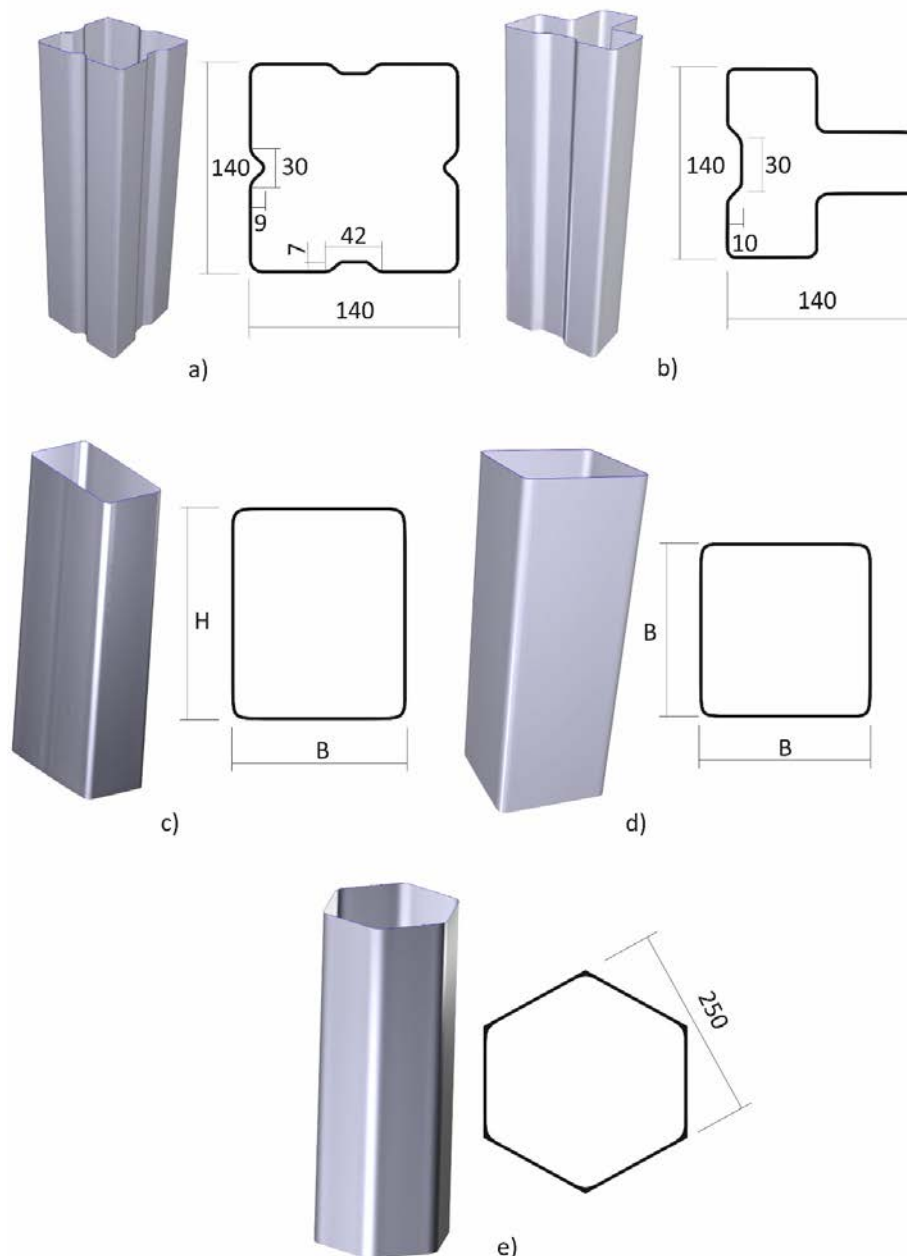


Figure 4: Studied cross-section types, made to EN 10210, EN 10219 or custom-made
a) square hollow section with stiffeners (SHS-S); b) square hollow section with stiffeners and T-shape (SHS-T); c) rectangular hollow sections (RHS); d) square hollow section (SHS); e) hexagonal hollow section (HEX).

As an example for the procedure employed at the different laboratories, Figure 5 gives a schematic representation of the test setup at Bundeswehr University Munich (BWU), shown here for the case of eccentrically loaded, short beam-columns. During the load application and up to and beyond the peak load, the test specimens were monitored through a combination of Digital Image Correlation (DIC) techniques and strain gauges and LVDTs. A typical representation of the DIC monitoring results is given in Figure 6.

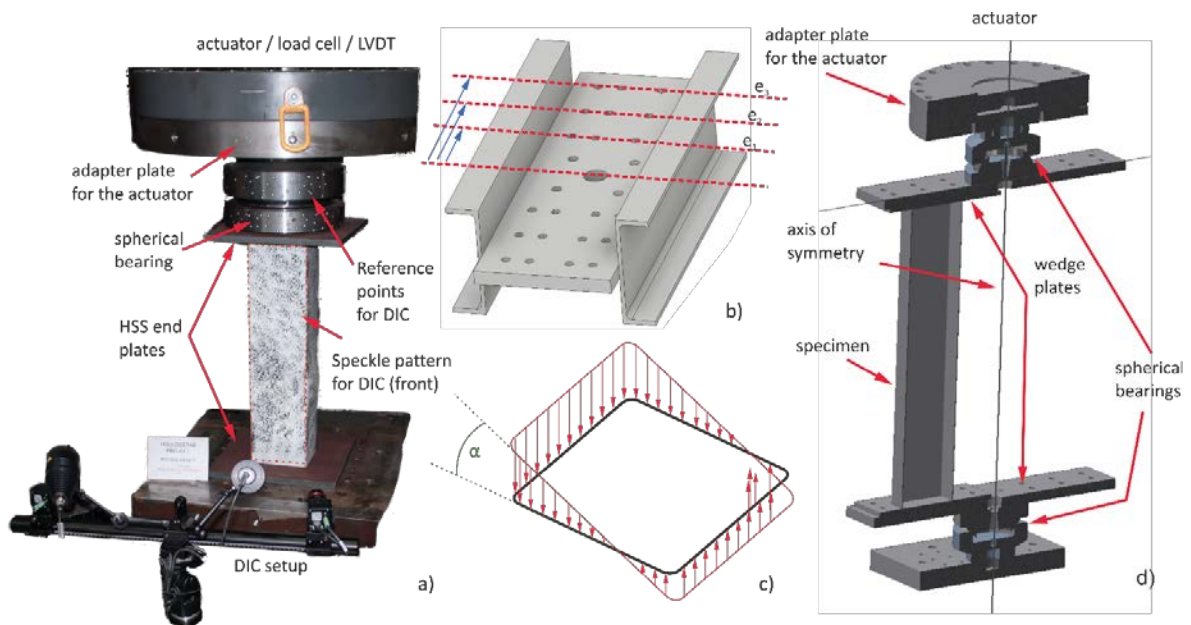


Figure 5: Schematic representation of the experimental test setup with interaction of axial force and bending moment; a) wedge plate used to introduce load eccentricities; b) induced elastic tensional; c) scheme of the test setup.

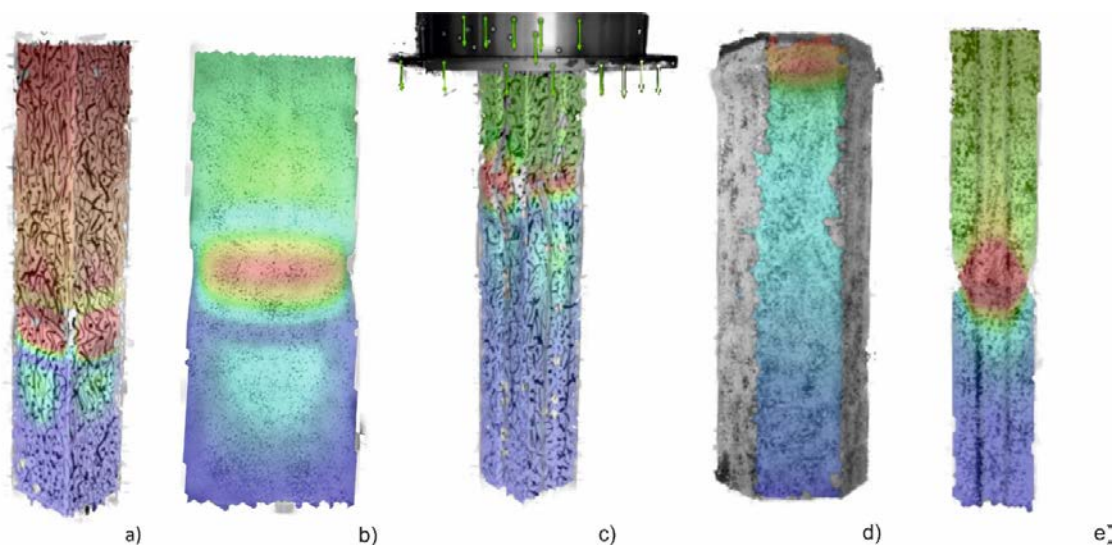


Figure 6: Failure modes for the stub column tests measured with the DIC system. The scale shows the maximum displacement in red and the minimum in blue; a) SHS, b) RHS, c) SHS-S, d) HEX, e) SHS-T

In the auxiliary tests and data collections, particular attention was paid to the accurate measurement of the actual geometrical shape of the tested specimens prior to load application, in particular with regards to local shape deviations (geometric imperfections), which are the main source of the on-set of local instability. 3D scanning techniques were used to determine this shape with accuracy of <0,1mm for the majority of tested specimens. A representative example of the documented shape deviations in the specimens tested at BWU is given in Figure 7.

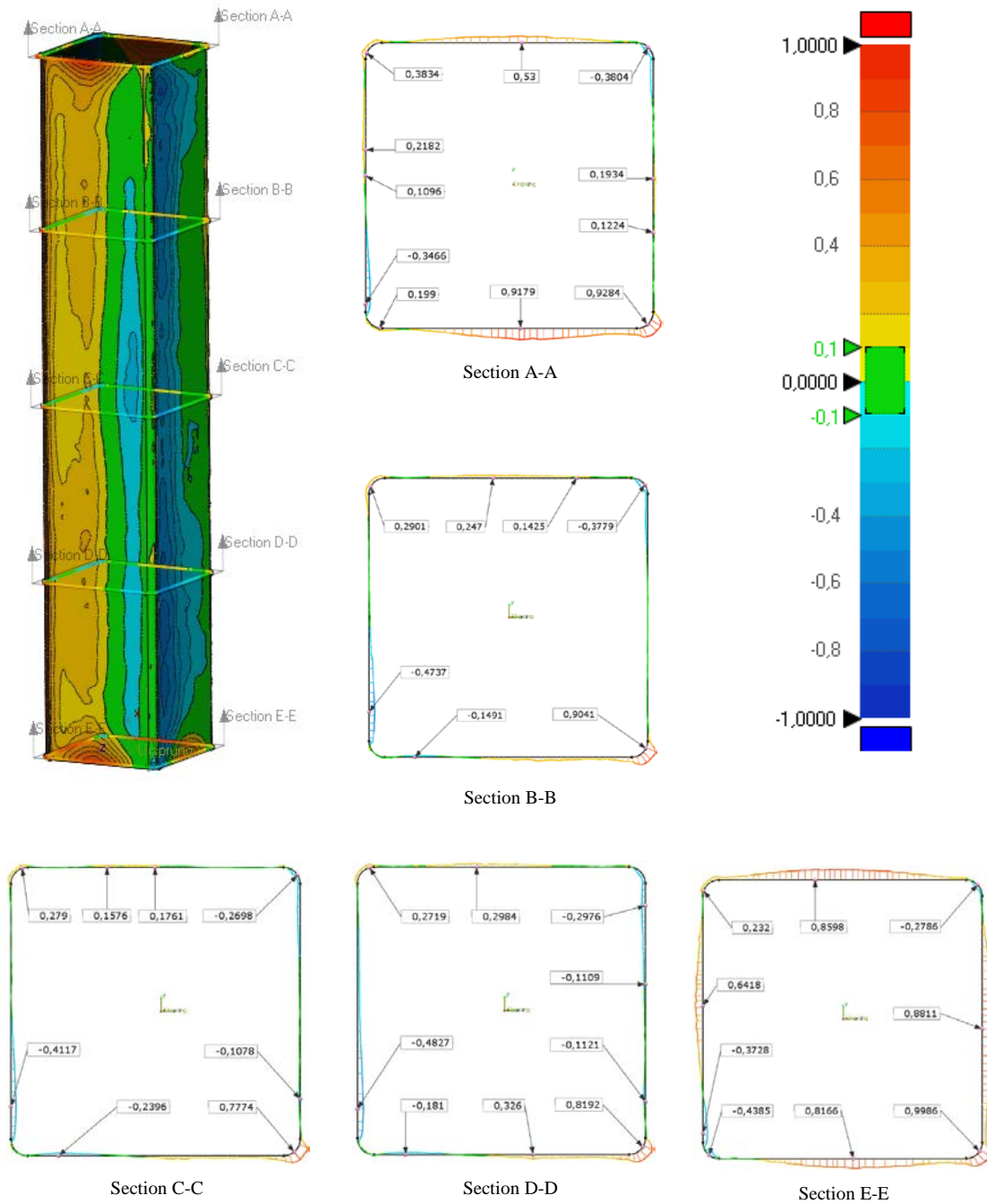


Figure 7: Example for shape deviations recorded through 3D scanning. SHS 140x140x4 cross section and S355 steel grade.

The physical tests were used as basis for the calibration of advanced, geometrically and materially non-linear FEM models and calculations, which account for material and geometric imperfections. These are referred to as “GMNIA” calculations. A representative example of the model calibration is given in Figure 8.

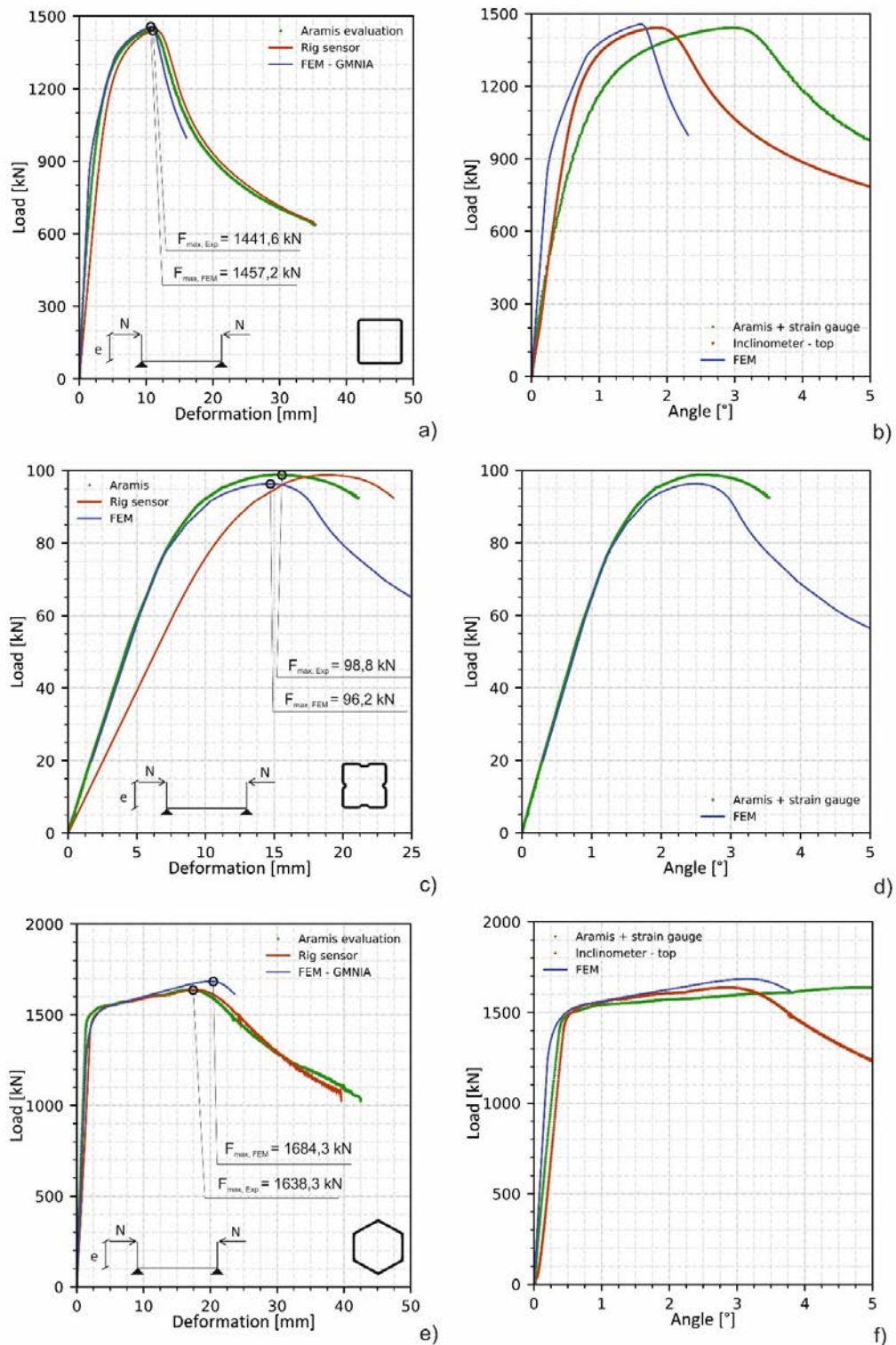


Figure 8: Exemplary results for the numerical (GMNIA) validation a) & b) SHS 200x200x8 S355; c) & d) SHS-S 140x140x2.5 S350GD; e) & f) HEX 250x8.5 S355 T3

Finally, the GMNIA models that were validated and verified against the physical tests and measured material and geometric properties (termed GMNIA-MEAS) were used as the basis for the calibration of more general GMNIA models for the extensive numerical parametric study, which used nominal geometric input data and scaled buckling eigenmodes. An example for the calibration of the finally chosen imperfection amplitudes for these models is shown in Figure 9.

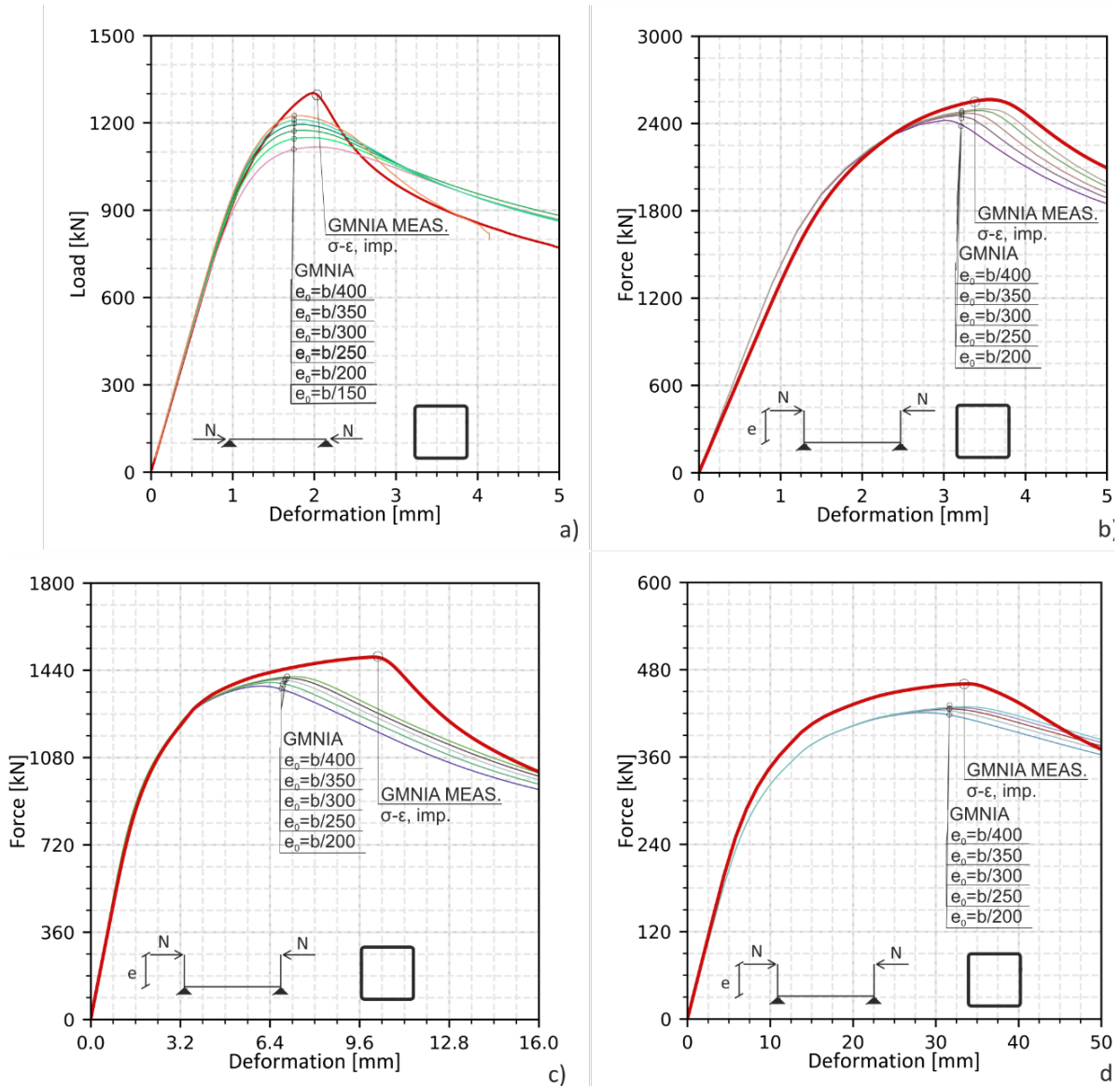


Figure 9: example calibration of the imperfection amplitude for the numerical parametric study for a) SHS 200x200x5 S355 T1-5, for b) SHS 200x200x8 S355 T2-3, for c) SHS 200x200x5 S355 T3-3 and for d) SHS 200x200x5 S355 T4-3.

The numerical parametric study for RHS and SHS sections comprised a total of more than 43,000 individual numerical tests, around 30,000 to study the cross-sectional capacity and around 13,000 to study the behavior of beam-columns, again loaded in a comprehensive number of combinations and compression and (bi-axial) bending and – in the case of beam-columns – of moment diagrams. The methodology used for this study, is schematically shown in Figure 10. Results are discussed in the context of the GSRM design rule validation in section 3.3. Further details are provided in the deliverables D4.2 [13] and D8.2 [16] of the *HOLLOSSTAB* project.

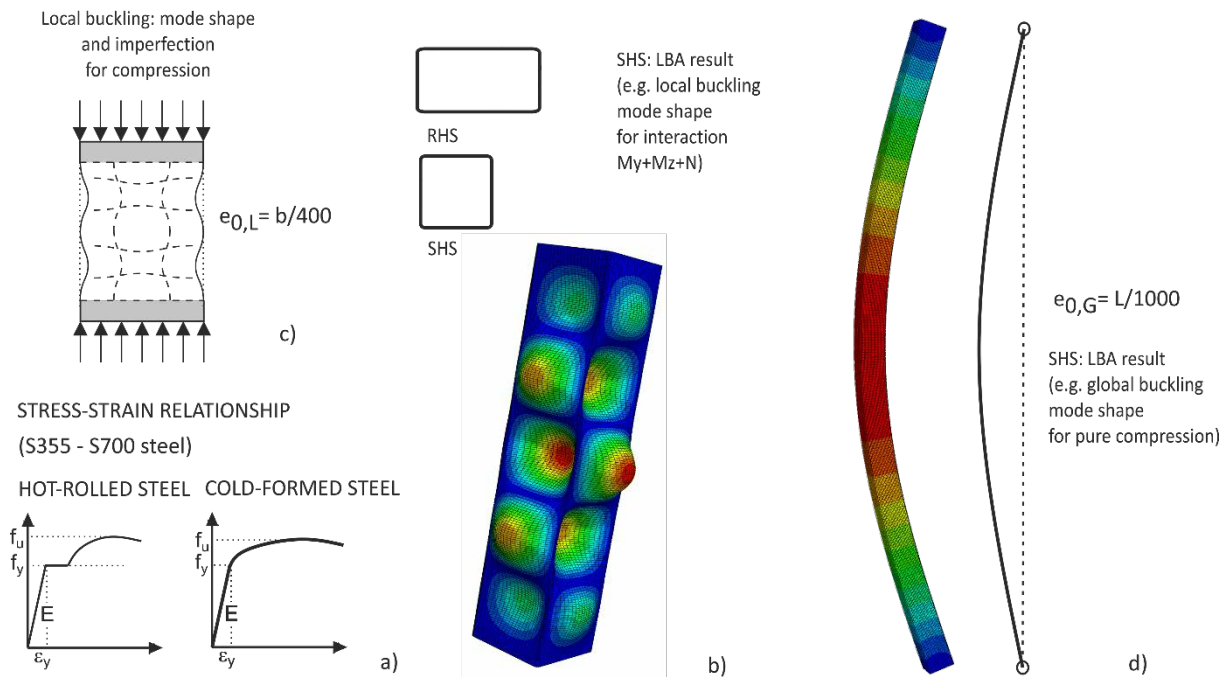
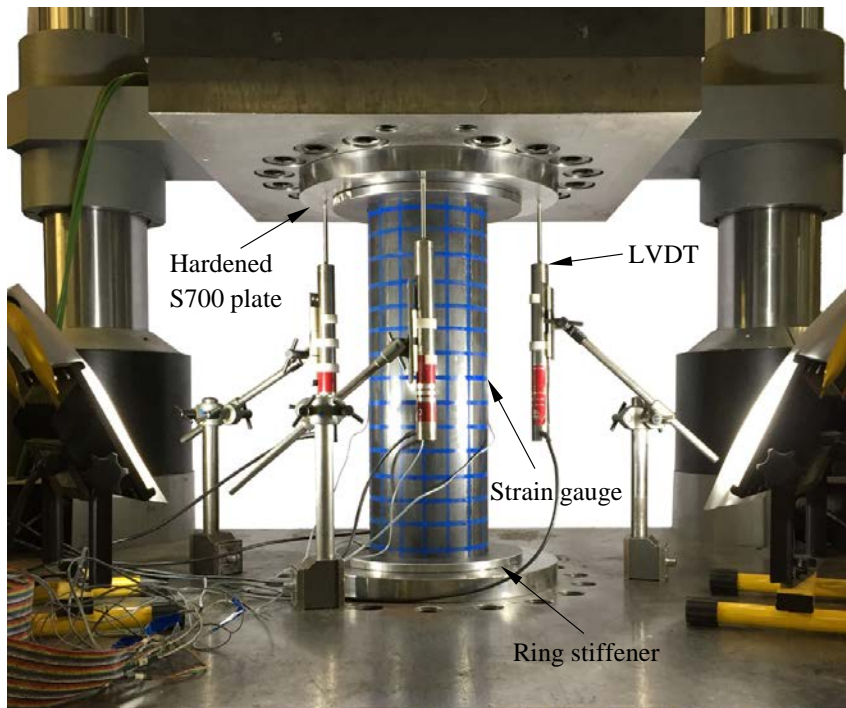


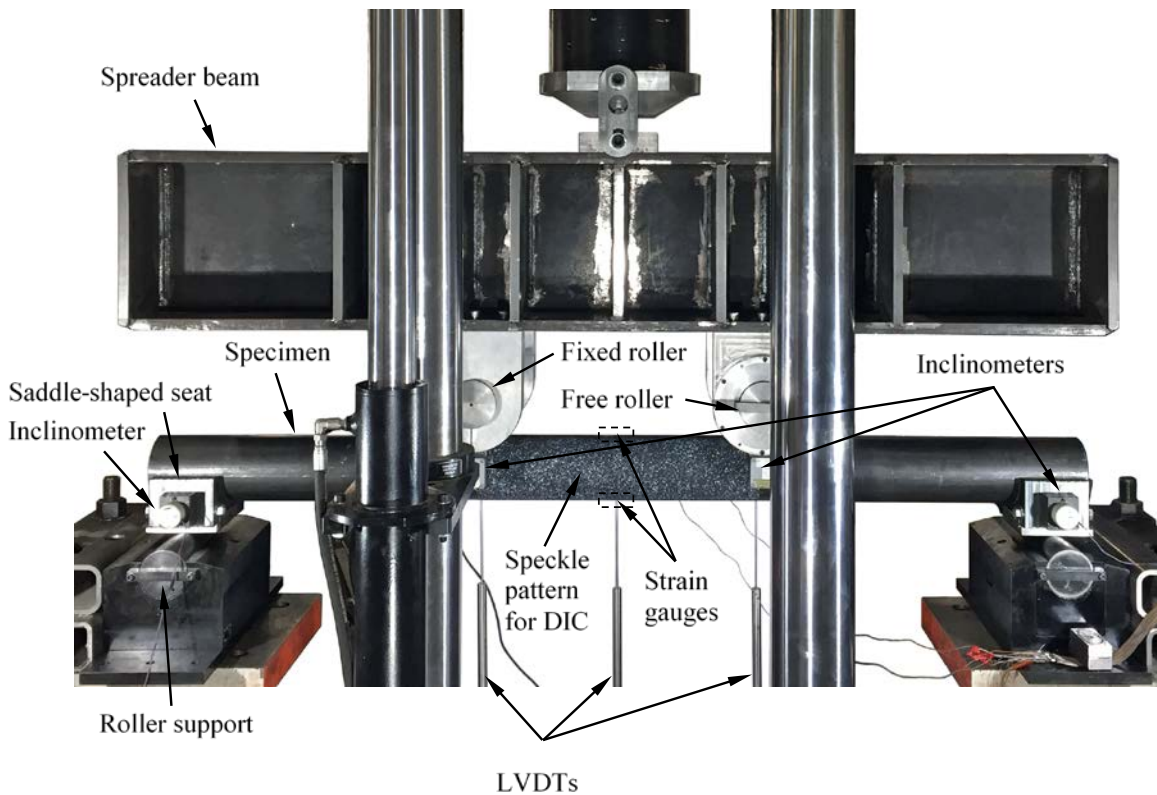
Figure 10: Methodology for the parametric study (RHS & SHS) a) Material model chosen for hot- and cold-formed sections; b) and d) LBA shape for the local imperfections; c) LBA shape for the local and d) global imperfections;

3.2.2 Cylindrical and Elliptical Hollow Sections (CHS/EHS)

A similarly comprehensive experimental programme to investigate the cross-sectional behaviour of circular hollow sections (CHS) was conducted during *HOLLOSSTAB*, see [14] and [17]. Thirteen circular hollow sections, including six cold-formed thermomechanically rolled S700 CHS, five hot-rolled S355 CHS and two cold-formed S355 CHS, were studied at Bundeswehr University Munich and Imperial College London. In total, 45 physical tests on CHS were performed, including twelve tensile coupon tests, thirteen stub column tests, twenty short beam-column tests, six four-point bending tests and six three-point bending tests, covering the load cases of axial compression, bending and the combination of both. Typical experimental test setups are demonstrated in Fig. 2, taken from the documentation of tests at Imperial College London (ICL). Further details and results of the experimental study on CHS are provided in the deliverable D3.2



(a) *Stub column test setup*



(b) *Four-point bending test setup*

Figure 11: *Experimental setups for CHS*

In parallel with the laboratory testing, a numerical simulation programme on the cross-sectional and member buckling behaviour of CHS and EHS was conducted. Finite element (FE) models for CHS and EHS were established and validated using the data generated from this project as well as those collected from the literature in terms of the ultimate loads, load-deformation histories and the failure modes; comparisons of typical load-deformation curves and failure modes are shown in Figs 3 and 4 respectively. Further details on the key modelling assumptions and the validation of the FE models are provided in D3.2; overall, the developed FE models were shown to be capable of accurately replicating the key experimental responses of CHS and EHS at both cross-section and member buckling levels.

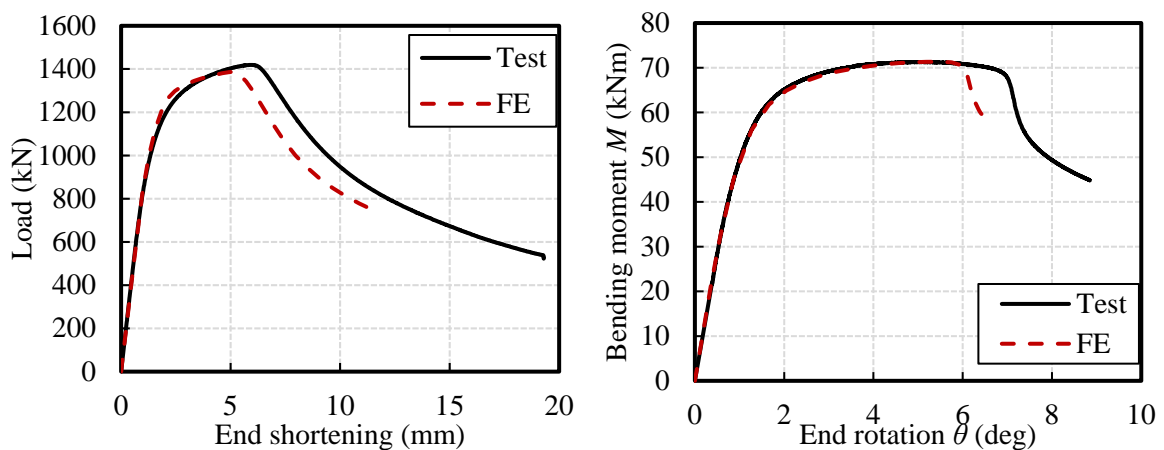


Figure 12: Typical experimental and numerical load-deformation curves for stub column tests (left) and four-point bending tests (right)



Figure 13: Typical experimental and numerical failure modes for stub column tests (left) and four-point bending tests (right)

Upon the validation of the FE models, parametric studies were conducted to generate numerical data for CHS and EHS to cover a wider range of cross-section aspect ratios, cross-section slendernesses, material grades, member lengths and load combinations. Both hot-rolled and cold-formed sections, with material grades spanning from S355 to S900, were examined in the parametric studies. In total, over 18000 additional structural performance data on CHS and EHS were numerically generated; these FE data were utilised in conjunction with the experimental results for the development and assessment of new design proposals.

3.3 Development and Calibration of Design Rules

The development of GSRM design rules was carried out for the individual failure modes by adhering to the structure of the intended design methodology as outlined in the following flowchart, see Figure 14. The following aspects were thereby considered:

- Four key factors are needed for the design checks of a hollow section that may fail in local and global buckling: the resistances “R” (in terms of load amplification factors) for the elastic buckling at the cross-sectional (local, $R_{cr,L}$) and member (global, $R_{cr,G}$) level, the elastic first-yield resistance R_{el} and the ideally-plastic resistance R_{pl} (yielding in every fibre)
- The cross-sectional capacity (“L” for local buckling) of all considered cross-sectional shapes is determined by multiplying the elastic resistance R_{el} by a buckling factor χ_L , which in turn is defined as a function of the local, cross-sectional slenderness $\bar{\lambda}_L = \sqrt{R_{el}/R_{cr,L}}$.
- The elastic range of the local buckling resistance is defined by a dedicated Winter-type [22] formulation for RHS/SHS respectively CHS/EHS.
- The plastic range (where a resistance higher than R_{el} may be achieved) may be determined by two alternative approaches:

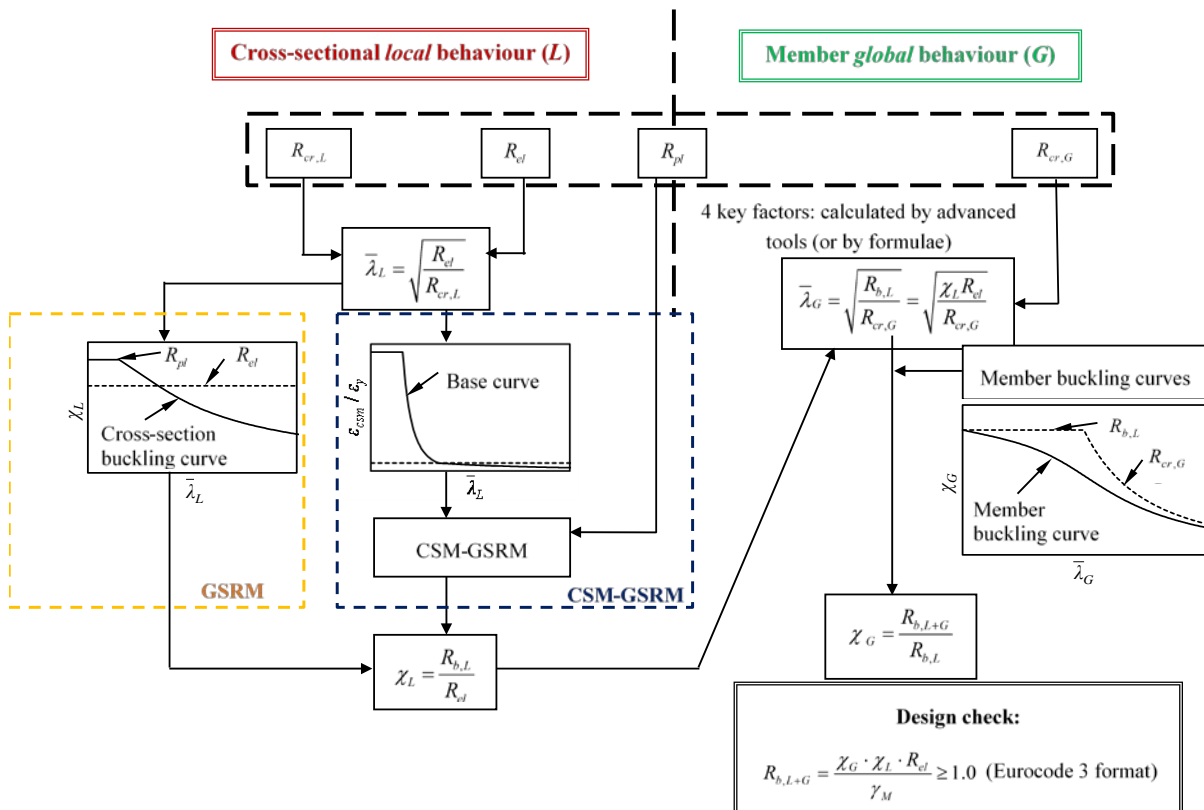


Figure 14: Flowchart of the GSRM for Local (L) and Global (G) buckling of hollow section columns and beam-columns

- A stress-based approach, which is simply termed “GSRM” in the flowchart. This approach has the advantage of great simplicity, yet does not provide nor require information about the strain level in the section at failure.
- A strain-based approach that is derived from a combination of the basic GSRM principles with those of the “Continuous Strength Method” (CSM), see [9]. This approach requires the evaluation of more complex resistance functions that account for the stress-strain relationships of the material, and thus differentiate more clearly between cold-formed and hot-finished sections. Strain hardening is accounted for explicitly, leading to more information about the stress-strain state of the section at failure and, often, to even more accurate results.
- Global buckling uses the resistance of the cross-section as basis for the definition of the global buckling factor and of the global slenderness $\bar{\lambda}_G = \sqrt{\chi_L \cdot R_{el}/R_{cr,L}}$. The GSRM-based buckling reduction factors were derived on the basis of second-order theory and the principles of the Ayrton-Perry approach, see also [7].

The full details on the development of the design rules may be found in D8.2 and D8.3 of the project ([16] and [17]), for RHS/SHS respectively CHS/EHS. Some key aspects and exemplary results are discussed in the following:

1. For the definition of the cross-sectional capacity, the spread of plasticity that sets on after the exceedance of the yield stress in the outermost fibre needed to be accounted for in the development of the design rules. For this reason, even though the GSRM eliminates the concept of cross-sectional classes as currently found in design codes, it is still necessary to distinguish between sections that may reach and exceed the elastic resistance R_{el} and those that will reach the peak load before this point. The development and calibration of new, GSRM-type design formulae for the cross-sectional strength of hollow sections was thus carried out for two distinct ranges: the elastic range, in which the local slenderness $\bar{\lambda}_L$ exceeded an elastic limit slenderness $\bar{\lambda}_0$, and the plastic range for smaller values of local slenderness.
2. the GSRM cross-sectional design rules for the elastic range were developed as modified Winter formulae, familiar from plate buckling cases as defined e.g. in [23], see also [24]. For all types of hollow section (rectangular, square, circular end elliptical), the following basic format was chosen for the definition of the buckling factor χ_L :

$$\chi_L = \left(1 - \frac{A}{\bar{\lambda}_L^{B_2}} \right) \frac{1}{\bar{\lambda}_L^{B_2}} \quad \text{for } \bar{\lambda}_L > \bar{\lambda}_0$$

In all cases, the coefficient A was used as a calibration factor. The power coefficient “B₁” was set to 1,0 in the case of RHS and SHS, while different values were used for CHS and EHS. One of the main factors influencing the values of these calibration coefficients was found to be the stress distribution within the section, represented by the coefficient $\psi = \sigma_{min}/\sigma_{max}$. For example, in the calibration of A for the design of RHS and SHS, it was seen to be conducive to good results to define A as a function ψ_1 and ψ_2 , i.e. the stress ratios in the two plates adjacent to the corner with the highest compressive stress in the section, see Figure 15.

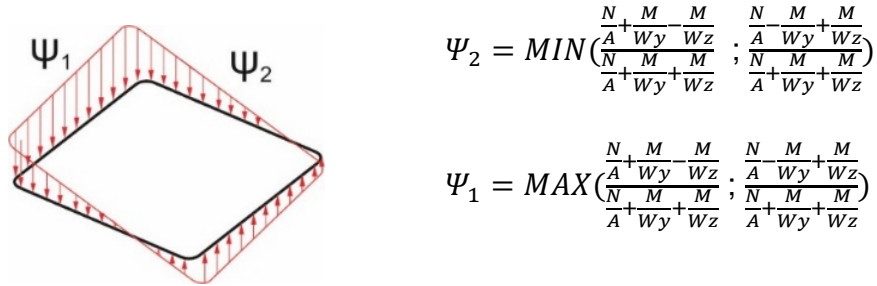


Figure 15: Definition and graphic representation of ψ_1 and ψ_2 as used in the GSRM formulation for the cross-sectional capacity of RHS and SHS

The following values of A were found to be best suited for an accurate and adequately safe representation of the buckling strength of RHS and SHS:

$$A = 0.225 + 0.025\psi_2 \frac{(1+\psi_1)}{2} \quad (\text{cold-formed sections})$$

$$A = 0.20 + 0.02\psi_2 \frac{(1+\psi_1)}{2} \quad (\text{hot-finished sections})$$

- As mentioned above, for the plastic (stocky) range two different formulations were developed in HOLLOSSTAB: a simplified bilinear function formulation and a method based on the Continuous Strength Method (CSM). The former is based on a simple expansion of the previously used, stress-based design to the stocky range, while the latter is a strain-based approach. The reader is referred to deliverable D8.3 [17] for details on the strain-based CSM-GSRM approach. The simplified, stress-based approach makes use of the following basic format:

$$\chi_L = 1 + (\alpha_{pl} - 1) \left(\frac{\bar{\lambda}_0 - \bar{\lambda}_L}{\bar{\lambda}_0 - \bar{\lambda}_{pl}} \right) \leq \alpha_{pl}$$

with the values for $\bar{\lambda}_{pl}$ and the maximum value α_{pl} calibrated to the data, separately for RHS/SHS respectively CHS/EHS.

- The accuracy of the design proposal for the cross-sectional capacity of RHS / SHS is illustrated in Figure 16 by means of comparison with the results of the GMNIA parametric study described in section 3.2 and with Eurocode design rules from prEN1993-1-1:2018.

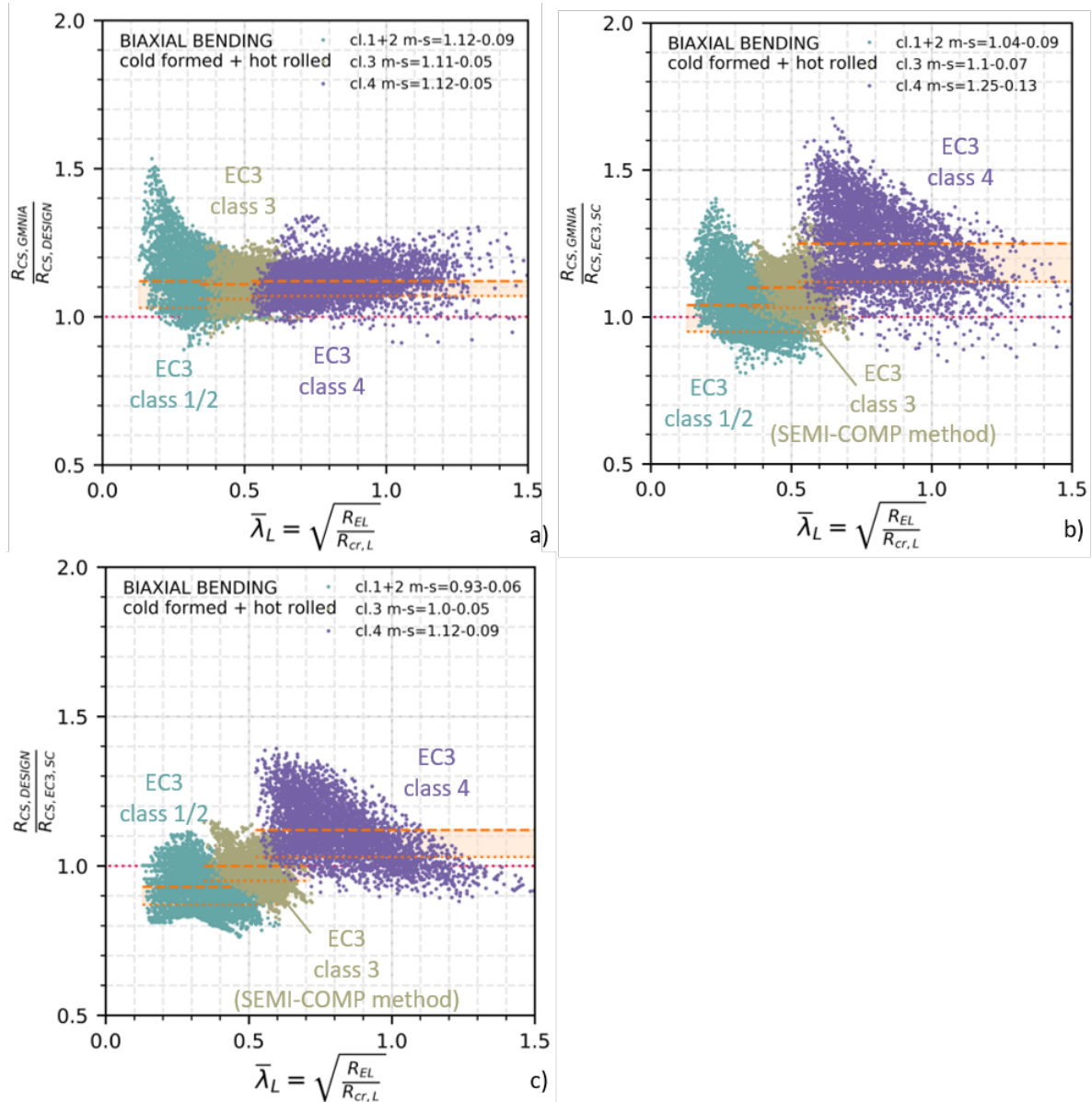


Figure 16: Validation of the GSRM rules vs. GMNIA and EC3 design rules for SHS and RHS: a) GMNIA results normalized by the GSRM results, plotted over slenderness; b) GMNIA vs. EC3 results; c) GSRM vs. EC3.

Gains in strength through the use of the GSRM compared to the current EC3 design strengths are particularly noticeable for class 4 sections. A - consciously accepted - lower resistance is found for class 1 and 2 sections, in order to compensate for an apparent lack of conservatism of the Eurocode rules in this range when compared to numerical (and physical) tests. However, it shall be noted that if this additional caution is not desired in a later implementation of the GSRM in a code-like design provision, this could be easily compensated by increasing the values of α_{pl} and $\bar{\lambda}_{pl}$. For EC3 class 3 sections, the methods are on average equivalent in their strength predictions. For high-strength steel sections, which almost exclusively fall in class 3 or (more often) 4, the gains in

strength were on average above 10%, and above 15% for class 4 sections. In cases with a pronounced level of bending biaxiality, the gains were even higher. In all cases, particularly those that involve load cases with combined compression and bending, the GSRM design method employs a much more straightforward design methodology and avoids the cumbersome determination and use of effective cross-sections (class 4 sections) respectively of multi-step design strengths for combined loading (class 1 to 3).

5. Similarly, the accuracy of the design proposal for the cross-sectional capacity of CHS / EHS is illustrated in Figure 17. Every dot in the figure represents a GMNIA result normalized by either the EC3 prediction (a) or the strength-based GSRM prediction (b) for CHS and EHS. The figure clearly shows that the GSRM yields significantly improved accuracy and consistency in the design predictions compared with the EC3 approach. On average, the GMNIA results lie higher than the strength-based GSRM by +19,9% for cold-formed CHS and +11,5% for hot-finished sections, with CoVs of 8,6% respectively 8,5%. The equivalent averages for the EC3 prediction are +39,7% (cold-formed) and +31,7% (hot-finished CHS), with COVs of 15,9% resp. 14,2%. Even better agreement with the GMNIA data is found by the strain-based CSM-GSRM approach.

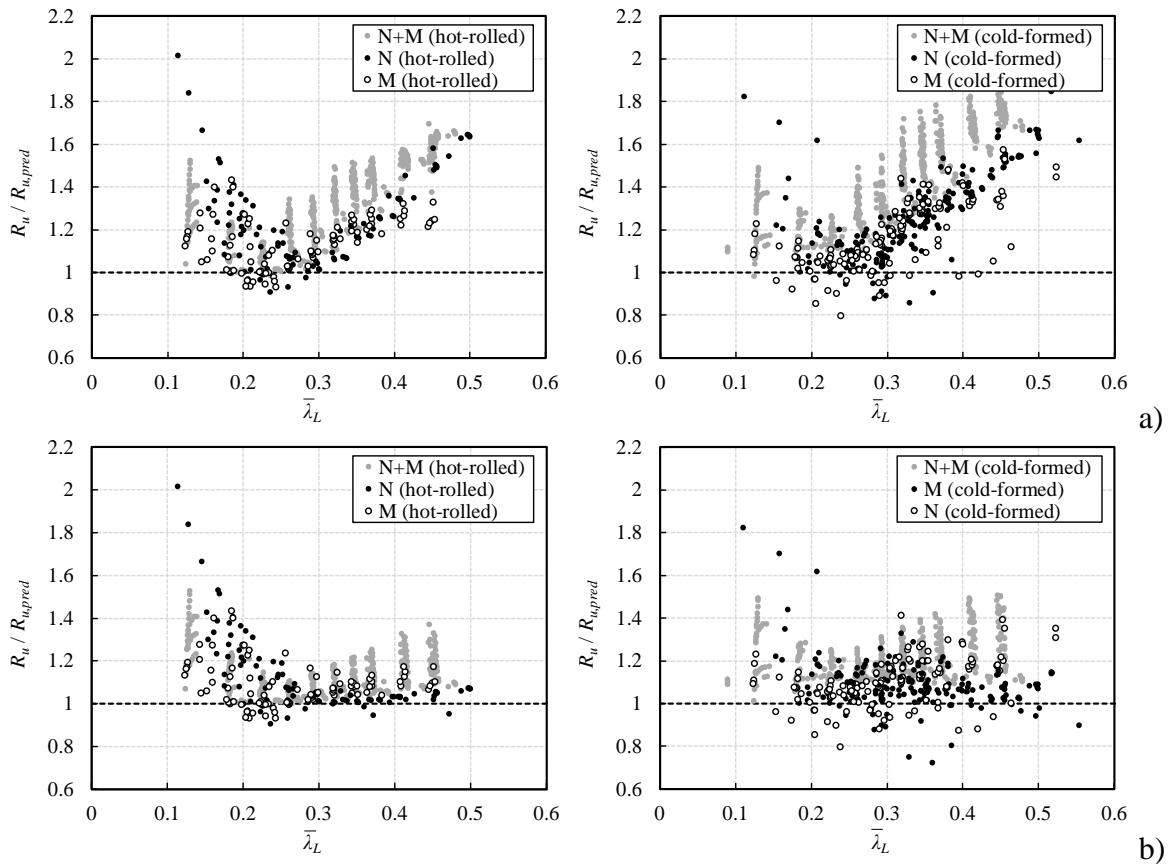


Figure 17: Comparisons of test and FE data on CHS with a) EC3 resistance predictions and b) resistance predictions from the strength-based GSRM

6. The design rules for members (global buckling) are based on a calibration of the so-called Ayrton-Perry formulation. This formulation for pure flexural buckling, valid for cases with pure and uniform compression, forms the basis for the steps taken in HOLLOSSTAB to derive specific GSRM-type rules for more general load cases in beam-columns with RHS or SHS section. The derivation of GSRM rules for members (beam-columns) was based to a large extent on second-order theory and basic mechanics. Only in a final step, some calibration factors were introduced to help adapt the mechanically derived formulation to the real, elasto-plastic non-linear behaviour as observed in physical and numerical tests.

The key factor governing the resistance of hollow section beam-columns, which fail in flexural buckling (but not in lateral-torsional buckling), is the relative eccentricity of loading. In compression members with internal eccentricities such as those given by an initial out-of-straightness, this is given by the amplitude e_0 of this shape deviation. In members loaded in compression and bending, this is represented by the ratio between the bending moments acting in the critical section and the compressive force. These quantities can be normalized by the section core width, respectively by the ratio between bending capacity $W_y f_y$ and compressive cross-sectional strength $A f_y$. For the in-plane case, this leads to the introduction of the following definitions η_{imp} and η_y .

$$\eta_{imp} = \frac{e_0 \cdot A f_y}{W_y f_y} \text{ and } \eta_y = \frac{\frac{M_y}{N}}{\frac{W_y f_y}{A f_y}}$$

These quantities were used in the derivation of the global (member) buckling rules for RHS/SHS and in one of the methods for CHS/SHS. The final result of the derivation of global buckling rules for hollow section beam-columns was a variation of the Ayrton-Perry formulation. For the in-plane case and the cross-sections mentioned above, it takes the following form:

$$\chi_G = \frac{1}{\Phi_G + \sqrt{\Phi_G^2 - \beta_{LG} \bar{\lambda}_G^2}}$$

$$\Phi_G = 0.5(\beta_{LG}(1 + \eta_{imp} + \eta_y) + \bar{\lambda}_G^2)$$

$$\text{with } \eta_{imp} = \alpha_{EC3}(\bar{\lambda}_G \sqrt{c_0} - 0.2) \text{ and } c_0 = (1 + \eta_y)$$

The coefficient β_{LG} describes the transitional behaviour in the elasto-plastic range for stockier cross-sections. This factor, as well as the expansion to a spatial buckling case, are described in detail in Deliverable D8.2 [16] of the project, and are presented in section 4 of these guidelines. The effectiveness of the approach is exemplified by the following two figures.

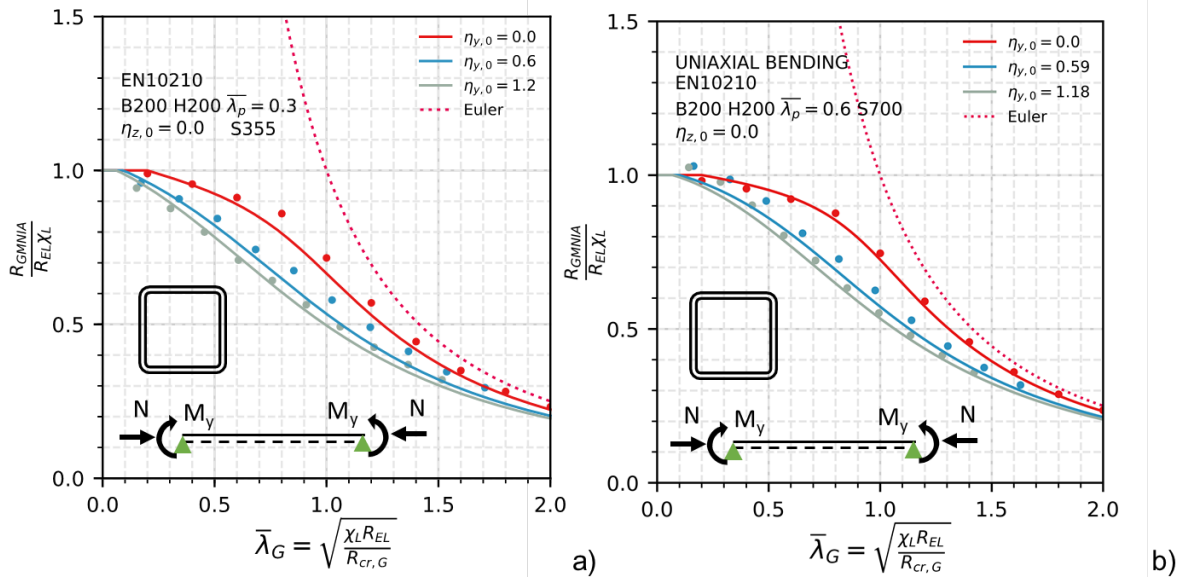


Figure 18: Comparison of GMNIA results (dots) and calibrated GSRM predictions (continuous lines) for various levels of eccentricity and hot-finished SHS with various plate thickness values; a) plate slenderness $\bar{\lambda}_p = 0.3$ (class 1 section); b) $\bar{\lambda}_p = 0.6$ (class 3 section)

Figure 18 shows that the behaviour of the GMNIA results is consistently described by the GSRM formulation. The left-sided part a) of this figure shows a class 1 SHS subjected to in-plane loading, with three different eccentricity levels and a uniform bending moment diagram. The points represent the GMNIA results in the $\bar{\lambda}_G - \chi_G$ plot, while the curve shows the corresponding buckling curve according to the developed and calibrated GSRM. In sub-plot b), similar results for a class 3 SHS subjected to in-plane loading are shown.

A more global view of the accuracy of the design rules for global buckling of RHS / RHS is given in the following Figure 19. The box plots give a graphical evaluation of the statistical parameters, with the area inside the box containing 50% of the data for a certain global slenderness, while the whiskers show the 5% upper and lower bound of the data and the “outliers” beyond this range are shown as small black points. In Figure 19a) and b), the results of the GMNIA numerical campaign on global buckling with constant bending moment along the member length are divided by the strength prediction of the new GSRM formulation for a) cold-formed sections and b) hot-finished sections. In Figure 19c) and d), the ratio between the GSRM prediction and the EC3 design value is shown. On average, the GSRM results are between 15% (hot-finished) and 10% (cold-formed sections) above the EC3 predictions for uniform bending diagrams. For non-uniform bending moment diagrams (Figure 19), the scatter is larger, yet the gains achieved by the GSRM are more significant, on average exceeding 20% for all types of section.

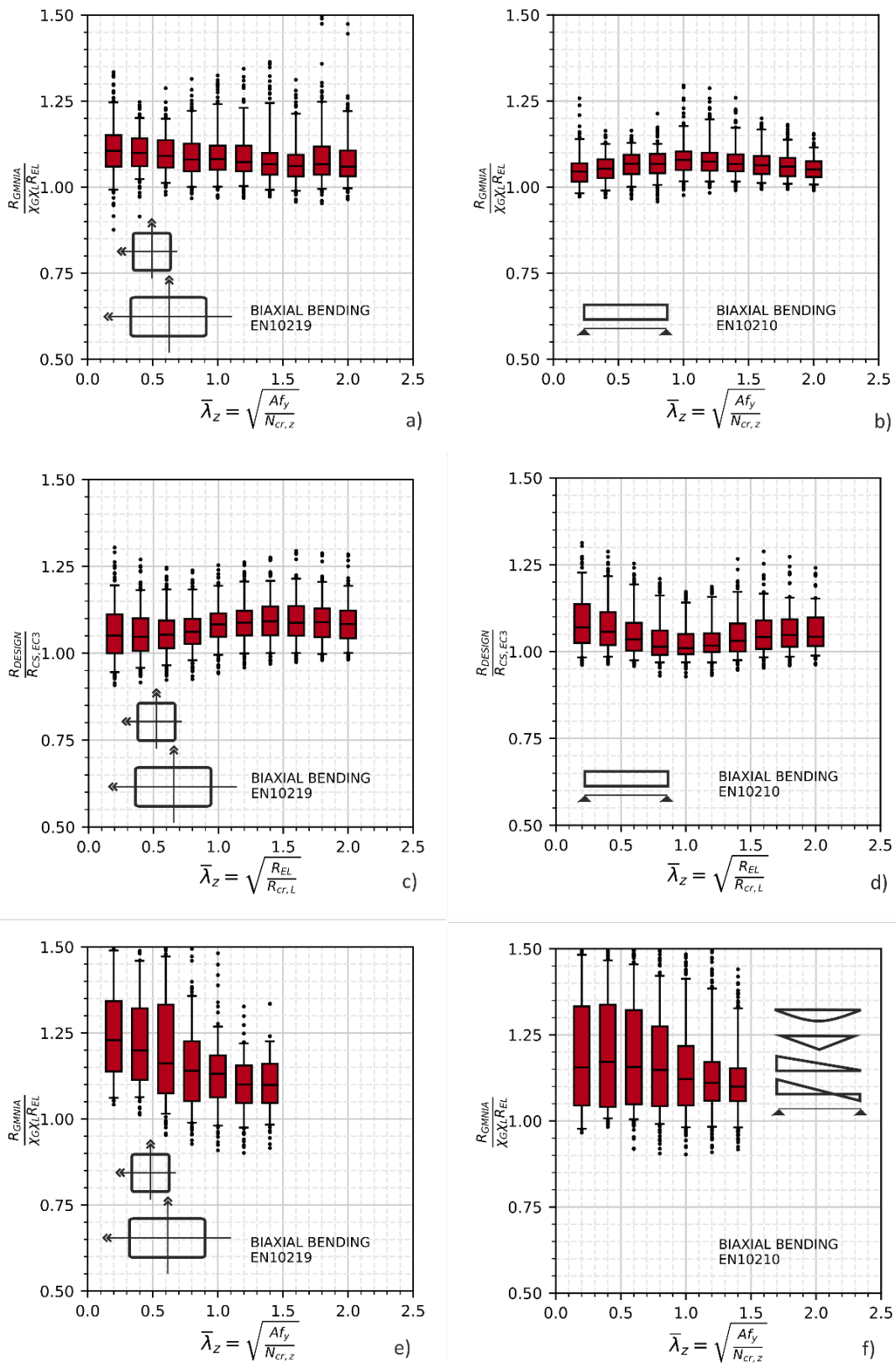


Figure 19: Box plots of: a) and b): GMNIA vs. GSRM, compression and biaxial uniform bending; c) and d): GSRM vs. EC3 rules, biaxial uniform bending; e) and f): GMNIA vs. GSRM, compression and various bending moment diagrams

7. Even higher gains were achieved for the global buckling of CHS (and EHS) beam-columns, see the comparison of the strength predictions of EC3 and of the proposed GSRM approach in Figure 20. While the new approach brings the scatter and conservatism in the same (low) range of the GSRM rules for RHS and SHS, the scatter of the current EC3 rules is very high. This is mainly due to the marked inaccuracy of the current ([2]) EC3 rules for CHS at the cross-sectional resistance level, which is carried over into the design of beam-columns. The elimination of the conservatism at the cross-sectional level given by the new GSRM approach is thus very beneficial for global buckling as well.

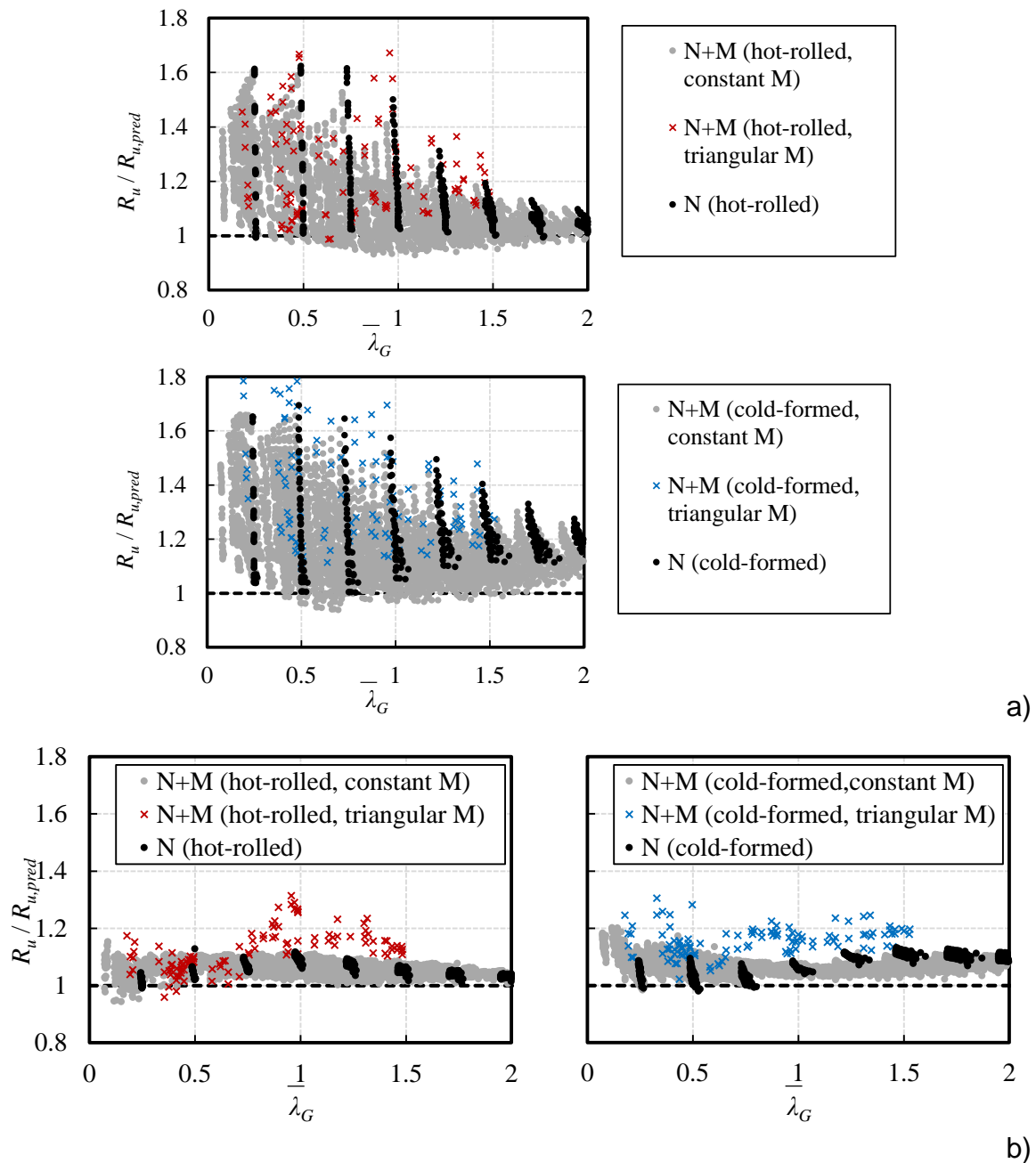


Figure 20: Comparisons of FEM (GMNIA) data on CHS with a) EC3 strength predictions and b) predicted resistances from proposed GSRM approach

- All design rules developed in *HOLLOSSTAB* were assessed with regards to their reliability using the methods provided of EN 1990 and further expanded and detailed during the RFCS project *SAFEBRICKTILE* ([25], [26]). The full details of these evaluations may be found in [18]. EC3-type partial factors of $\gamma_M=1,0$ were found to be sufficiently safe and accurate when used in combination with the GSRM design rules for both the cross-sectional and global (member) buckling resistances developed in *HOLLOSSTAB*.

3.4 Software Tool

A dedicated design software that allows for a direct and practical calculation of all input parameters and slenderness values of the GSRM and directly leads to the postulated design strength of the method was developed by *HOLLOSSTAB* project partners at CTICM and at the University of Lisbon (see [19]).

The development of the software was split in two parts. First, algorithms and programs were developed to numerically determine the main input parameters of the GSRM method, i.e. the elastic and plastic as well as the critical (buckling) load amplification factor. These programs represent the calculation core implemented into the Graphical User Interface (GUI) developed in the second part of this development task. The GUI allows the user to define step-by-step their design configuration and to visualise directly the main results in the “Result” tab. Additionally, the user has the possibility to generate a calculation sheet that may be printed or saved in .pdf format. The following two figures (Figure 21 and Figure 22) show screen shots of the GUI.

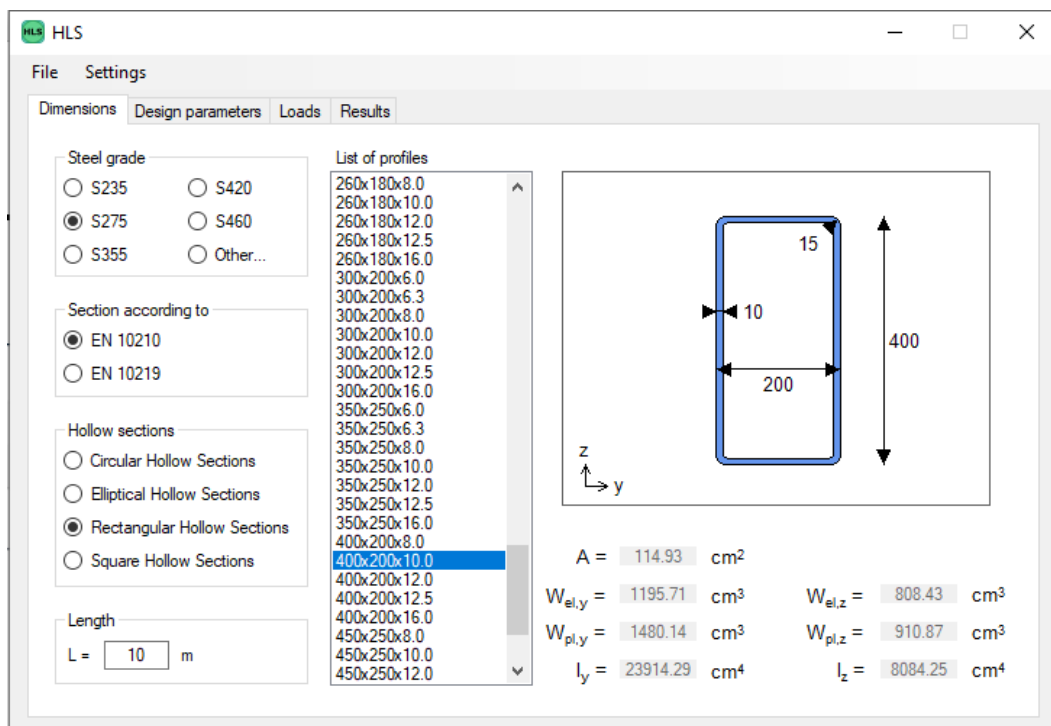


Figure 21: Main tab of the Graphical User Interface

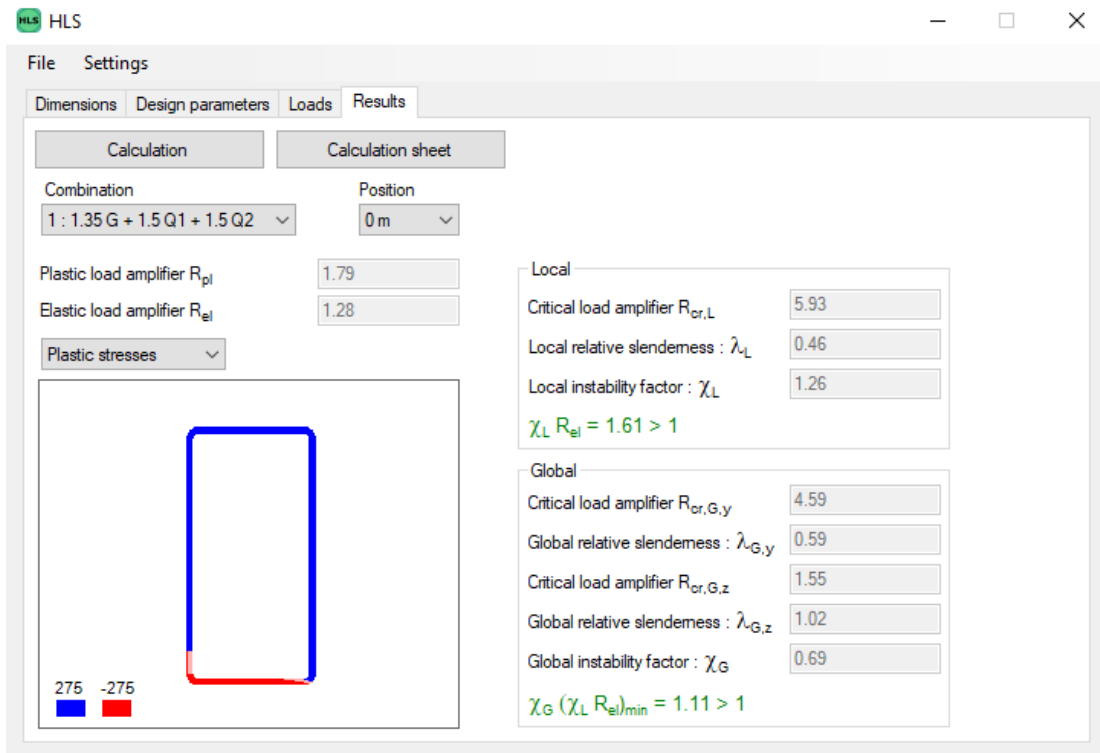


Figure 22: Result tab of the Graphical User Interface

The GUI has been developed using the language VB.net for Windows operating systems from Windows 7 to Windows 10. The piece of software is delivered to the end user as a setup package that will be available free of charge. By running this setup package, the software will be installed on the hard disk of the user's computer. The software has been designed as multi-lingual allowing the use to choose between French and English.

After the final approval of the project in early 2020 by RFCS, this software will be made available to the public through the homepage of the European Convention for Constructional Steelwork (ECCS – www.steelconstruct.com/eu-projects/hollosstab).

4 DESIGN RECOMMENDATION

The following pages contain a summary of the design recommendations and proposals for GSRM design rules developed in *HOLLOSSTAB*.

4.1 Recommendations for Cross-Sectional Capacity Checks

4.1.1 Common definitions

1. Cross-sectional strength R_L :

$$R_{b,L} = R_{el} \cdot \chi_L$$

with:

$R_{b,L}$... load amplifier to reach the cross-sectional resistance

R_{el} ... load amplifier to reach compressive first yield in the section

χ_L buckling coefficient to account for elastic or plastic local buckling

2. Cross-sectional slenderness:

$$\bar{\lambda}_L = \sqrt{\frac{R_{el}}{R_{cr,L}}}$$

3. Cross-section check: $\frac{R_{b,L}}{\gamma_{M0}} \geq 1$

with $\gamma_{M0}=1,0$.

4.1.2 GSRM rules for RHS/SHS

1. Elastic-plastic slenderness limit:

$$\bar{\lambda}_0 = 0.5 + \sqrt{0.25 - A}$$

2. Buckling coefficient χ_L - elastic range

$$\text{for } \bar{\lambda}_L > \bar{\lambda}_0 \quad \chi_L = \left(1 - \frac{A}{\bar{\lambda}_L}\right) \cdot \frac{1}{\bar{\lambda}_L}$$

$$A = (0.2 + 0.02\psi_2) \frac{(1+\psi_1)}{2} \quad \text{for hot-finished sections}$$

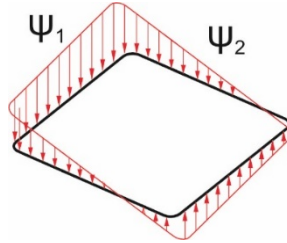
$$A = (0.225 + 0.025\psi_2) \frac{(1+\psi_1)}{2} \quad \text{for cold-formed sections}$$

Where ψ_1 and ψ_2 are defined as follows:

$$\psi_1 = \text{MAX} \left(\frac{\frac{N}{A} + \frac{M}{W_y}}{\frac{M}{W_z}} ; \frac{\frac{N}{A} + \frac{M}{W_y}}{\frac{M}{W_z}} \right)$$

$$\Psi_2 = \text{MIN} \left(\frac{\frac{N}{A} + \frac{M}{W_y} - \frac{M}{W_z}}{\frac{N}{A} + \frac{M}{W_y} + \frac{M}{W_z}} ; \frac{\frac{N}{A} - \frac{M}{W_y} + \frac{M}{W_z}}{\frac{N}{A} + \frac{M}{W_y} + \frac{M}{W_z}} \right)$$

Ψ_1 and Ψ_2 are the stress ratios in the two plates adjacent to the corner with the highest compressive stress in the section.



1. Buckling coefficient χ_L – plastic range – Approach 1 (stress-based)

$$\text{for } \bar{\lambda}_L \leq \bar{\lambda}_0 \quad \chi_L = 1 + (\alpha_{pl} - 1) \cdot \frac{\bar{\lambda}_0 - \bar{\lambda}_L}{\bar{\lambda}_0 - 0,3} \leq \min(\alpha_{pl}; 1,5)$$

with:

$$\alpha_{pl} = \frac{R_{pl}}{R_{el}}$$

4.1.3 GSRM rules for CHS/EHS

1. Local elastic slenderness limit:

$$\bar{\lambda}_0 = 0.43 - 0.07 \left(\frac{1 + \psi}{2} \right)^2$$

where

$$\psi = \frac{\frac{N_{Ed}}{N_{pl}} - \frac{M_{y,Ed}}{M_{el,y}} - \frac{M_{z,Ed}}{M_{el,z}}}{\frac{N_{Ed}}{N_{pl}} + \frac{M_{y,Ed}}{M_{el,y}} + \frac{M_{z,Ed}}{M_{el,z}}}$$

2. Buckling coefficient - elastic range

for $\bar{\lambda}_0 < \bar{\lambda}_L \leq 0.6$:

$$\chi_L = \left(1 - \frac{A}{\bar{\lambda}_L^{B_2}} \right) \frac{1}{\bar{\lambda}_L^{B_2}}$$

where

$$A = \left(1 - \bar{\lambda}_0^{-B_2} \right) \bar{\lambda}_0^{-B_2}$$

$$B_2 = 0.3$$

3. Buckling coefficient – plastic range -Approach 1 (stress-based)

for $\bar{\lambda}_L \leq \bar{\lambda}_0$:

$$\chi_L = 1 + (\alpha_{pl} - 1) \frac{\bar{\lambda}_0 - \bar{\lambda}_L}{\bar{\lambda}_0 - 0.25} \leq \min(1.5, \alpha_{pl})$$

where

$$\alpha_{pl} = \frac{R_{pl}}{R_{el}}$$

4.1.4 Alternative rules for CHS/EHS in the plastic range - CSM/GSRM approach

In the stocky range, where $\bar{\lambda}_L \leq \bar{\lambda}_0$, an alternative deformation (strain) based cross-section design approach is developed for CHS and EHS on the basis of the Continuous Strength Method (CSM) to exploit the benefits from the spread of plasticity and strain hardening. The proposed design procedure is set out as follows:

1. Local slenderness:

$$\bar{\lambda}_L = \sqrt{\frac{R_{el}}{R_{cr,L}}} = \sqrt{\frac{f_y}{f_{cr}}}$$

2. Local slenderness limits:

$$\bar{\lambda}_0 = 0.43 - 0.07 \left(\frac{1 + \psi}{2} \right)^2$$

where

$$\psi = \frac{\frac{N_{Ed}}{N_{pl}} - \frac{M_{y,Ed}}{M_{el,y}} - \frac{M_{z,Ed}}{M_{el,z}}}{\frac{N_{Ed}}{N_{pl}} + \frac{M_{y,Ed}}{M_{el,y}} + \frac{M_{z,Ed}}{M_{el,z}}}$$

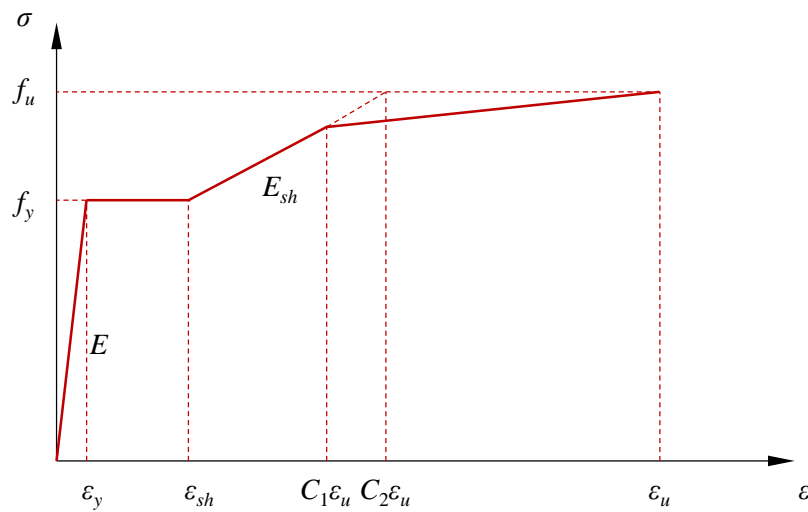
3. Base curves:

$$\frac{\varepsilon_{csm}}{\varepsilon_y} = \left(\frac{\bar{\lambda}_0}{\bar{\lambda}_L} \right)^{B_1} \leq \min \left(15, \frac{C_1 \varepsilon_u}{\varepsilon_y} \right) \text{ for } \bar{\lambda}_L \leq \bar{\lambda}_0$$

$$B_1 = 2.5 + \left(\frac{1 + \psi}{2} \right)^2$$

4. Material models:

For hot-rolled steels:



$$E_{sh} = \frac{f_u - f_y}{C_2\epsilon_u - \epsilon_{sh}}$$

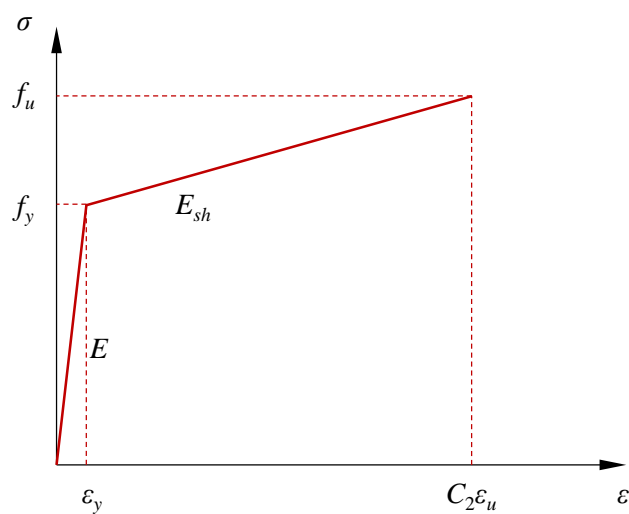
$$\epsilon_{sh} = 0.1 \frac{f_y}{f_u} - 0.055, \text{ but } 0.015 \leq \epsilon_{sh} \leq 0.03$$

$$\epsilon_u = 0.6 \left(1 - \frac{f_y}{f_u} \right) \text{ but } \epsilon_u \geq 0.06$$

$$C_1 = \frac{\epsilon_{sh} + 0.25(\epsilon_u - \epsilon_{sh})}{\epsilon_u}$$

$$C_2 = \frac{\epsilon_{sh} + 0.4(\epsilon_u - \epsilon_{sh})}{\epsilon_u}$$

For cold-formed steels:



$$E_{sh} = \frac{f_u - f_y}{C_2\epsilon_u - \epsilon_y}$$

$$\varepsilon_u = 0.6 \left(1 - \frac{f_y}{f_u} \right)$$

$$C_1 = 0.4 ; C_2 = 0.45$$

5. Resistance functions:

For hot-rolled hollow sections:

$$R_{b,L} = R_{csm} = R_{pl} \left(1 - \left(1 - \frac{R_{el}}{R_{pl}} \right) / \left(\frac{\varepsilon_{csm}}{\varepsilon_y} \right)^2 + 0.1 \left(\frac{\varepsilon_{csm} - \varepsilon_{sh}}{\varepsilon_y} \right)^2 \frac{E_{sh}}{E} \right) \quad \text{for } \varepsilon_{csm} > \varepsilon_{sh}$$

$$R_{b,L} = R_{csm} = R_{pl} \left(1 - \left(1 - \frac{R_{el}}{R_{pl}} \right) / \left(\frac{\varepsilon_{csm}}{\varepsilon_y} \right)^2 \right) \quad \text{for } \varepsilon_y < \varepsilon_{csm} \leq \varepsilon_{sh}$$

For cold-formed hollow sections:

$$R_{b,L} = R_{csm} = R_{pl} \left(1 - \left(1 - \frac{R_{el}}{R_{pl}} \right) / \left(\frac{\varepsilon_{csm}}{\varepsilon_y} \right)^2 + \frac{E_{sh}}{E} \frac{R_{el}}{R_{pl}} \left(\frac{\varepsilon_{csm}}{\varepsilon_y} - 1 \right) \right)$$

4.1.5 Alternative rules for RHS/SHS in the plastic range - CSM/GSRM approach

The equivalent CSM-GSRM approach for the cross-sectional design of stocky RHS and SHS is governed by the following, additional equations:

1. Base curve:

$$\frac{\varepsilon_{csm}}{\varepsilon_y} = \left(\frac{\bar{\lambda}_0}{\bar{\lambda}_L} \right)^{B_1} \leq \min \left(15, \frac{C_1 \varepsilon_u}{\varepsilon_y} \right) \quad \text{for } \bar{\lambda}_L \leq \bar{\lambda}_0$$

2. Resistance functions:

- *For hot-finished sections:*

$$R_{csm} = R_{pl} \left[1 - \frac{\left(1 - \frac{R_{el}}{R_{pl}} \right)}{\left(\frac{\varepsilon_{csm}}{\varepsilon_y} \right)^2} + 0.1 \left(\frac{\varepsilon_{csm} - \varepsilon_{sh}}{\varepsilon_y} \right)^2 \frac{E_{sh}}{E} \right] \quad \text{for } \varepsilon_{csm} > \varepsilon_{sh}$$

$$R_{csm} = R_{pl} \left[1 - \frac{\left(1 - \frac{R_{el}}{R_{pl}} \right)}{\left(\frac{\varepsilon_{csm}}{\varepsilon_y} \right)^2} \right] \quad \text{for } \varepsilon_y < \varepsilon_{csm} \leq \varepsilon_{sh}$$

$$R_{csm} = R_{el} \frac{\varepsilon_{csm}}{\varepsilon_y} \quad \text{for } \bar{\lambda}_L > \bar{\lambda}_0$$

- *For cold-formed sections:*

$$R_{csm} = R_{pl} \left[1 - \frac{\left(1 - \frac{R_{el}}{R_{pl}} \right)}{\left(\frac{\varepsilon_{csm}}{\varepsilon_y} \right)^2} + 0.1 \left(\frac{\varepsilon_{csm} - \varepsilon_y}{\varepsilon_y} \right)^2 \frac{E_{sh}}{E} \frac{R_{el}}{R_{pl}} \right] \quad \text{for } \bar{\lambda}_L \leq \bar{\lambda}_0$$

$$R_{csm} = R_{el} \frac{\varepsilon_{csm}}{\varepsilon_y} \quad \text{for } \bar{\lambda}_L > \bar{\lambda}_0$$

4.2 Recommendations for Member Buckling Checks

The following pages contain formulae and tables summarizing the global (member) buckling design rules for RHS/SHS and CHS/EHS. For the latter, two slightly different approaches were developed in *HOLLOSSTAB*. The first approach accounts for some peculiarities of cylindrical sections, such as the fact that the point of maximum stress can be at various locations when the cross-sections are bent about two axes, by making use of the stress ratio $\psi = \sigma_{\min} / \sigma_{\max}$ for the whole section, instead of using the normalized load eccentricity for the principal axes η_y and η_z as previously described. This leads to slightly better accuracy in some load cases. The second approach for CHS/EHS strives for the maximum compatibility with the case of RHS and SHS, thus achieving a unified set of rules for all hollow section beam-columns.

4.2.1 Common definitions

Cross-section resistance: $R_{b,L}$, $\chi_L = \frac{R_{b,L}}{R_{el}}$

Global slenderness $\bar{\lambda}_G$:

$$\bar{\lambda}_G = \sqrt{\frac{R_{b,L,\min}}{R_{cr,G}}}$$

Design value of the global buckling strength:

$$R_{b,G} = \chi_G R_{b,L,\min} = \chi_G \cdot \chi_L \cdot R_{el}$$

Design check:

$$\frac{R_{b,G}}{\gamma_{M1}} \geq 1 \quad \text{with } \gamma_{M1} = 1,0$$

4.2.2 GSRM rules for RHS/SHS and CHS/EHS (Approach 2)

These rules are summarized in the forms of tables in the following pages.

4.2.3 GSRM rules for CHS/EHS (Approach 1)

1. Local-global modification factor β_{LG} :

$$\beta_{LG} = \left(1 - \left(1 - \frac{1}{\chi_L} \right) / k \right) \leq 1$$

$$\text{where } k = \left(\frac{R_{cr,G}}{R_{b,L}} \right)^{0.25} = \frac{1}{\sqrt{\bar{\lambda}_G}} \geq 1$$

2. Global buckling reduction factor χ_G :

$$\chi_G = \frac{\beta_{LG}}{\phi + \sqrt{\phi^2 - \beta_{LG} \bar{\lambda}_G^2}} \quad \text{but } \chi_G \leq \beta_{LG}$$

where

$$\eta = \alpha \left(\sqrt{\beta_{LG} \cdot \bar{\lambda}_G} - \bar{\lambda}_0 \right)$$

$$\phi = 0.5 \left(1 + \eta + \beta_{LG} \bar{\lambda}_G^2 \right)$$

$$\bar{\lambda}_0 = 0.2$$

$$\alpha = 0.3(1 - \psi) + 0.6\varepsilon \quad \text{for cold-formed CHS \& EHS}$$

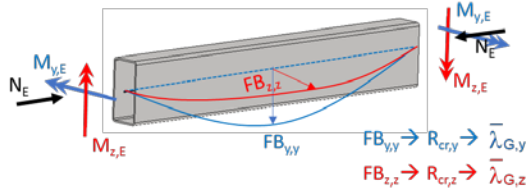
$$\alpha = 0.35(1 - \psi) + 0.26\varepsilon \quad \text{for hot-rolled CHS \& EHS}$$

$$\varepsilon = \sqrt{\frac{235}{f_y}}$$

$$\psi = \frac{\frac{N_{Ed}}{N_{pl}} - \frac{C_{my} M_{y,Ed}}{M_{el,y}} - \frac{C_{mz} M_{z,Ed}}{M_{el,z}}}{\frac{N_{Ed}}{N_{pl}} + \frac{C_{my} M_{y,Ed}}{M_{el,y}} + \frac{C_{mz} M_{z,Ed}}{M_{el,z}}}$$

Note: for spatial cases, it is conservatively assumed that global instability about the minor axis always governs, and $M_{y,Ed}$ is taken as 0 when calculating ψ

DESIGN RECOMMENDATIONS



Proposals for global buckling – RHS /SHS

COMMON SYMBOLS FOR ALL BUCKLING DIRECTIONS

$$R_{b,L} = \chi_L R_{el}$$

$$\alpha_{EC3} = 0,21 \text{ (hot-finished, S235 to S420)}$$

$$\alpha_{EC3} = 0,13 \text{ (hot-finished, S460 and higher)}$$

$$\alpha_{EC3} = 0,49 \text{ (cold-formed) // } 0,34 \text{ for S460 and higher}$$

$$M_{el,y} = W_{el,y} f_y$$

$$M_{el,z} = W_{el,z} f_y$$

$$N_{el} = A f_y$$

$$\eta_y = \frac{\frac{M_{y,E,max}}{N_E}}{\frac{N_{el}}{N_E}} ; \quad \eta_z = \frac{\frac{M_{z,E,max}}{N_E}}{\frac{N_{el}}{N_E}}$$

$$c_0 = 1 + \eta_y + \eta_z$$

ξ_{LG} : for $\chi_L \leq 1,0$: $\xi_{LG} = 1$
 for $\chi_L > 1,0$: $\xi_{LG} = 1 + (\chi_L - 1) \cdot \rho \cdot \bar{\lambda}_{G,y} \cdot C_m \leq \chi_L$
 with $\rho = 0,5$ for cold-formed; $\rho = 0,6$ for hot-finished sections

$$\beta_{LG} = \frac{\xi_{LG}}{c_0}$$

Moment diagram	C_m
	1.0
	0.95
	0.9
	$0.6 + 0.4\psi_M$

FB-y-y: 2nd order effect mostly in z-direction

$$N_{cr,y} = \frac{\pi^2 EI_y}{L^2} \quad R_{cr,y} = \frac{N_{cr,y}}{N_e} \quad \bar{\lambda}_{G,y} = \sqrt{\frac{R_{b,L,min}}{R_{cr,y}}} \quad \beta_{LG,y} = \frac{\xi_{LG,y}}{c_0}$$

with $\xi_{LG,y}$: for $\chi_L \leq 1,0$: $\xi_{LG,y} = 1$

for $\chi_L > 1,0$: $\xi_{LG,y} = 1 + (\chi_L - 1) \cdot \rho \cdot \bar{\lambda}_{G,y} \cdot C_{m,y} \leq \chi_L$

FB-z-z: 2nd order effect mostly in y-direction

$$N_{cr,z} = \frac{\pi^2 EI_z}{L^2} \quad R_{cr,z} = \frac{N_{cr,z}}{N_e} \quad \bar{\lambda}_{G,z} = \sqrt{\frac{R_{b,L,min}}{R_{cr,z}}} \quad \beta_{LG,z} = \frac{\xi_{LG,z}}{c_0}$$

with $\xi_{LG,z}$: for $\chi_L \leq 1,0$: $\xi_{LG,z} = 1$

for $\chi_L > 1,0$: $\xi_{LG,z} = 1 + (\chi_L - 1) \cdot \rho \cdot \bar{\lambda}_{G,z} \cdot C_{m,z} \leq \chi_L$

$$\chi_{G,y} = \frac{1}{\Phi_{G,y} + \sqrt{\Phi_{G,y}^2 - \beta_{LG,y} \cdot \bar{\lambda}_{G,y}^2}} \leq 1,0$$

$$\Phi_{G,y} = \frac{1}{2} \left[\beta_{LG,y} (1 + \eta_z C_{m,z} + \eta_y C_{m,y} + \eta_{EC3,y}) + \bar{\lambda}_{G,y}^2 \right]$$

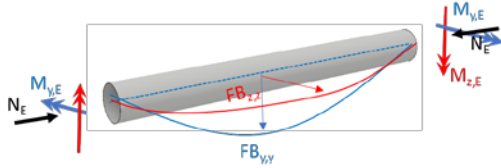
$$\eta_{EC3,y} = \alpha_{EC3} (\bar{\lambda}_{G,y} \sqrt{c_0} - 0,2)$$

$$\chi_{G,z} = \frac{1}{\Phi_{G,z} + \sqrt{\Phi_{G,z}^2 - \beta_{LG,z} (1 + \eta_y C_{m,y}) \bar{\lambda}_{G,z}^2}} \leq 1,0$$

$$\Phi_{G,z} = \frac{1}{2} \left[\beta_{LG,z} (1 + \eta_z C_{m,z} + \eta_y C_{m,y} + \eta_{EC3,z}) + \bar{\lambda}_{G,z}^2 \right]$$

$$\eta_{EC3,z} = \alpha_{EC3} (\bar{\lambda}_{G,z} \sqrt{c_0} - 0,2)$$

$$\chi_G = \text{MIN}(\chi_{G,y}; \chi_{G,z}) \quad R_{b,G+L} = \chi_G \cdot \chi_L \cdot R_{el}$$



Proposals for global buckling – CHS /EHS (Approach 2)

COMMON SYMBOLS FOR ALL BUCKLING DIRECTIONS

$$R_{b,L} = \chi_L R_{el}$$

$$\alpha_{EC3} = 0,26\varepsilon \text{ (hot-finished)}$$

$$\alpha_{EC3} = 0,60\varepsilon \text{ (cold-formed)}$$

$$k_{CS} = 1,1$$

$$M_{el,y} = W_{el,y} f_y^*$$

$$M_{el,z} = W_{el,z} f_y^*$$

$$N_{el} = A f_y$$

* for CHS, a vector addition of the two moments may be applied for CHS, leading to an in-plane problem

$$\eta_y = \frac{\frac{M_{y,E,max}}{M_{el,y}}}{\frac{N_E}{N_{el}}} \quad ; \quad \eta_z = \frac{\frac{M_{z,E,max}}{M_{el,z}}}{\frac{N_E}{N_{el}}}$$

$$c_0 = 1 + \eta_y + \eta_z$$

ξ_{LG} :

for $\chi_L \leq 1,0$: $\xi_{LG} = 1$
 for $\chi_L > 1,0$: $\xi_{LG} = 1 + (\chi_L - 1) \cdot \rho \cdot \bar{\lambda}_{G,y} \cdot C_m \leq \chi_L$
 with $\rho = 1,4$ for cold-formed; $\rho = 1,6$ for hot-finished sections

$$\beta_{LG} = \frac{\xi_{LG}}{c_0}$$

Moment diagram	C_m
	1.0
	0.95
	0.9
M $\psi_M M$	$0.6 + 0.4\psi_M$

FB-y-y: 2nd order effect mostly in z-direction

$$N_{cr,y} = \frac{\pi^2 EI_y}{L^2} \quad R_{cr,y} = \frac{N_{cr,y}}{N_e} \quad \bar{\lambda}_{G,y} = \sqrt{\frac{R_{b,L,min}}{R_{cr,y}}} \quad \beta_{LG,y} = \frac{\xi_{LG,y}}{c_0}$$

with $\xi_{LG,y}$: for $\chi_L \leq 1,0$: $\xi_{LG,y} = 1$
 for $\chi_L > 1,0$: $\xi_{LG,y} = 1 + (\chi_L - 1) \cdot \rho \cdot \bar{\lambda}_{G,y} \cdot C_{my} \leq \chi_L \cdot k_{CS}$

FB-z-z: 2nd order effect mostly in y-direction

$$N_{cr,z} = \frac{\pi^2 EI_z}{L^2} \quad R_{cr,z} = \frac{N_{cr,z}}{N_e} \quad \bar{\lambda}_{G,z} = \sqrt{\frac{R_{b,L,min}}{R_{cr,z}}} \quad \beta_{LG,z} = \frac{\xi_{LG,z}}{c_0}$$

with $\xi_{LG,z}$: for $\chi_L \leq 1,0$: $\xi_{LG,z} = 1$
 for $\chi_L > 1,0$: $\xi_{LG,z} = 1 + (\chi_L - 1) \cdot \rho \cdot \bar{\lambda}_{G,z} \cdot C_{mz} \leq \chi_L \cdot k_{CS}$

$$\chi_{G,y} = \frac{1}{\Phi_{G,y} + \sqrt{\Phi_{G,y}^2 - \beta_{LG,y} \cdot \bar{\lambda}_{G,y}^2}} \leq 1,0$$

$$\Phi_{G,y} = \frac{1}{2} \left[\beta_{LG,y} (1 + \eta_z C_{m,z} + \eta_y C_{m,y} + \eta_{EC3,y}) + \bar{\lambda}_{G,y}^2 \right]$$

$$\eta_{EC3,y} = \alpha_{EC3} (\bar{\lambda}_{G,y} \sqrt{c_0} - 0,2)$$

$$\chi_{G,z} = \frac{1}{\Phi_{G,z} + \sqrt{\Phi_{G,z}^2 - \beta_{LG,z} (1 + \eta_y C_{m,y}) \bar{\lambda}_{G,z}^2}} \leq 1,0$$

$$\Phi_{G,z} = \frac{1}{2} \left[\beta_{LG,z} (1 + \eta_z C_{m,z} + \eta_y C_{m,y} + \eta_{EC3,z}) + \bar{\lambda}_{G,z}^2 \right]$$

$$\eta_{EC3,z} = \alpha_{EC3} (\bar{\lambda}_{G,z} \sqrt{c_0} - 0,2)$$

$$\chi_G = \text{MIN}(\chi_{G,y}; \chi_{G,z}) \quad R_{b,G+L} = \chi_G \cdot \chi_L \cdot R_{el}$$

5 WORKED EXAMPLES

Several worked examples are presented in this chapter, for various hollow sections under different loading conditions. Several steel grades are taken into consideration, including high-strength steel. There are cases of local, cross-sectional resistance as well as beam-columns. The chosen examples cover the entire range of cross-section classes according to the prEN-1993-1-1:2018.

Each example is calculated using the current Draft standard of the Eurocode 3 revision, prEN-1993-1-1:2018, as the basis of comparison with EC3 . A FEM calculation using a Geometrically and Materially Nonlinear Analysis with Imperfections (GMNIA) was used as a reference case for all examples, using the commercial software SIMULIA ABAQUS. The modelling techniques concerning the FEM discretization and the material characterization are described in detail in Deliverables D3.2 and D4.3 of the HOLLOSSTAB project ([14], [13]).

In all examples, the resistances were compared at the characteristic level, i.e. without consideration of any partial factor γ_M . This was done to avoid entering this parameter as an additional term in the comparisons. It shall however be noted that γ_{M0} and $\gamma_{M1} = 1,0$ were validated to be applicable for the GSRM design rules developed in HOLLOSSTAB, see section 3.3.

5.1 Example 1 - Cross-Sectional Capacity, RHS 250x150x5, EN10219, S700

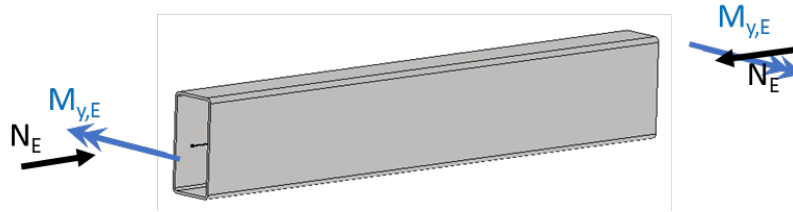


Figure 23: Schematic representation of the cross-section with applied load

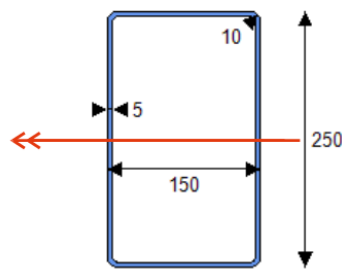


Figure 24: Cross-section dimensions with bending moment

$$A = 38.36 \text{ cm}^2$$

$$I_y = 3304 \text{ cm}^4$$

$$W_{y,el} = 264 \text{ cm}^3$$

$$W_{y,pl} = 320 \text{ cm}^3$$

$$I_z = 1508 \text{ cm}^4$$

$$W_{z,el} = 201 \text{ cm}^3$$

$$W_{z,pl} = 225 \text{ cm}^3$$

Load

$$N_{Ed} = 550 \text{ kN}$$

$$M_{y,Ed} = 120 \text{ kNm}$$

5.1.1 Design according to EC3

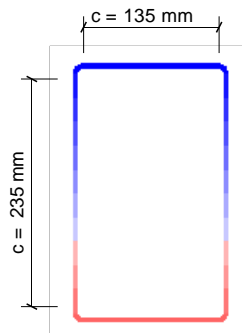


Figure 25: Elastic stress distribution, with c values for the purposes of classification

Maximum width-to-thickness ratios for compression parts (sheet 1 of 3)
[Table 7.3 of prEN1993-1-1:2018]

Internal compression parts			
Key: 1: Axis of bending			
Stress distribution in parts (compression positive)			
Class 1	$c/t \leq 72 \varepsilon$	$c/t \leq 28 \varepsilon$	when $\alpha_c > 0,5$: $c/t \leq \frac{126 \varepsilon}{5,5 \alpha_c - 1}$ when $\alpha_c \leq 0,5$: $c/t \leq \frac{36 \varepsilon}{\alpha_c}$
Class 2	$c/t \leq 83 \varepsilon$	$c/t \leq 34 \varepsilon$	when $\alpha_c > 0,5$: $c/t \leq \frac{188 \varepsilon}{6,53 \alpha_c - 1}$ when $\alpha_c \leq 0,5$: $c/t \leq \frac{41,5 \varepsilon}{\alpha_c}$
Stress distribution in parts (compression positive)			
Class 3	$c/t \leq 121 \varepsilon$	$c/t \leq 38 \varepsilon$	when $\psi > -1$: $c/t \leq \frac{38 \varepsilon}{0,608 + 0,343 \psi + 0,049 \psi^2}$ when $\psi \leq -1^*$: $\frac{c}{t} \leq 60,5 \varepsilon (1 - \psi)$

The reduction factor for the flange is as follows:

$$\bar{\lambda}_p = \frac{c_{flange}}{28.4 \varepsilon \sqrt{k_\sigma}} = 0.82$$

$$\rho = \frac{\bar{\lambda}_p - 0.055(3 + \psi)}{\lambda_p^2} = 0.89$$

The resulting section modulus is then:

$$W_{y,eff} = 251 \text{ cm}^3$$

For the calculation of the effective area, we assume both flange and web in full compression ($k_\sigma = 4.0$, $\psi = 1.0$).

$$\lambda_p = \frac{c_{flange}}{28.4 \varepsilon \sqrt{k_\sigma}} = 0.82$$

$$\rho_{flange} = \frac{\lambda_p - 0.055(3 + \psi)}{\lambda_p^2} = 0.89$$

$$\lambda_p = \frac{c_{web}}{28.4 \varepsilon \sqrt{k_\sigma}} = 1.43$$

$$\rho_{web} = \frac{\lambda_p - 0.055(3 + \psi)}{\lambda_p^2} = 0.59$$

And the effective area finally:

$$A_{eff} = 26.55 \text{ cm}^2$$

The goal is to evaluate the load amplification factor.

$$R_{EC3} \cdot \left(\frac{N_{Ed}}{A_{eff} f_y} + \frac{M_{yEd}}{W_{y,el} f_y} \right) = 1.0$$

$$R_{EC3} = 1.022$$

$$U_{EC3} = \frac{1}{R_{EC3}} = 0.979$$

5.1.2 *HOLLOSSTAB* design method

The software “HLS” developed for the *HOLLOSSTAB* project will be used to determine the values needed for the calculation of the amplification factor $R_{L,HS}$.

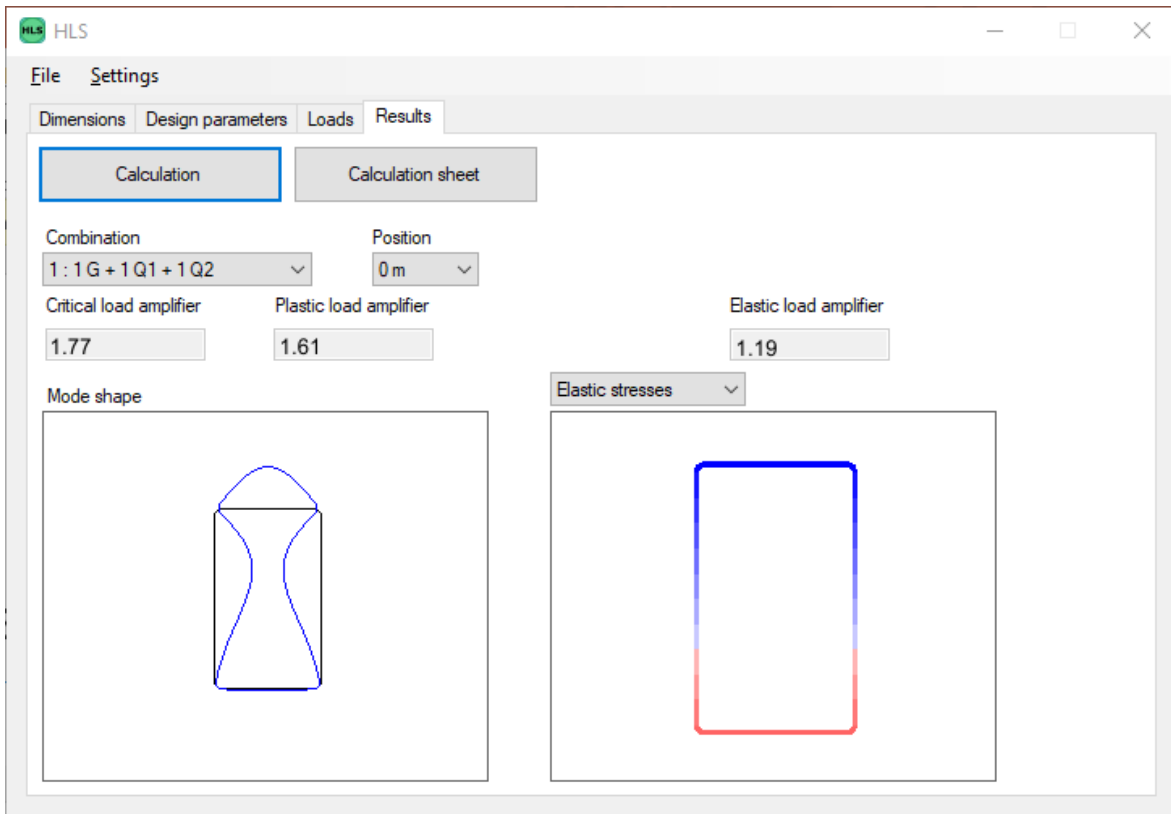


Figure 26: The “Results” window of the HLS software

$$R_{el} = 1.19$$

$$R_{cr} = 1.77$$

$$\bar{\lambda}_L = \sqrt{R_{el}/R_{cr}} = 0.821$$

$$R_{pl} = 1.61$$

It is necessary to calculate the elastic stresses distribution in the cross-section under combined load, to find the highest and the second highest value of ψ .

$$\psi_1 = MAX \left(\frac{N}{A} + \frac{M}{W_y} ; \frac{N}{A} - \frac{M}{W_y} \right)$$

$$\psi_2 = MIN \left(\frac{N}{A} + \frac{M}{W_y} ; \frac{N}{A} - \frac{M}{W_y} \right)$$

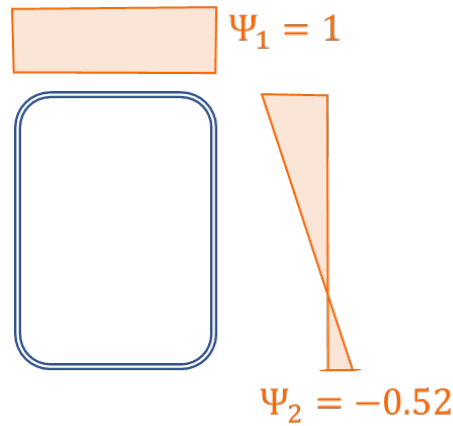


Figure 27: Graphical representation of the ψ values

$$B_2 = 1$$

$$A = (0.225 + 0.025\psi_2) \frac{(1 + \psi_1)}{2} = 0.212$$

$$\bar{\lambda}_0 = 0.5 + \sqrt{0.25 - A} = 0.695$$

for $\bar{\lambda}_L > \bar{\lambda}_0$:

$$\chi_L = \left(1 - \frac{A}{\bar{\lambda}_L^{B_2}}\right) \cdot \frac{1}{\bar{\lambda}_L^{B_2}} = 0.904$$

$$R_{L,HS} = R_{el} \cdot \chi_L = 1.19 \cdot 0.904 = 1.077$$

5.1.3 Summary of results

$$R_{EC3} = 1.022$$

$$R_{L,HS} = 1.077$$

$$R_{GMNIA} = 1.188$$

$$U_{EC3} = \frac{1}{R_{EC3}} = 0.979$$

$$U_{L,HS} = \frac{1}{R_{L,HS}} = 0.929$$

$$U_{GMNIA} = \frac{1}{R_{GMNIA}} = 0.842$$

$$\frac{R_{L,HS}}{R_{EC3}} = 1.054$$

The results show that the cross-sectional resistance prediction of the new GSRM method is 5,4% higher than the current Eurocode design methodology for the studied section, while still being around 10% on the safe side compared to the realistic GMNIA resistance.

5.2 Example 2 - Cross-Sectional Capacity, RHS 180x120x8, EN10210, S460

This example will show a case of hot finished RHS of at least class 2, according to the EC3. This cross-section is loaded in compression and both major and minor axis bending.

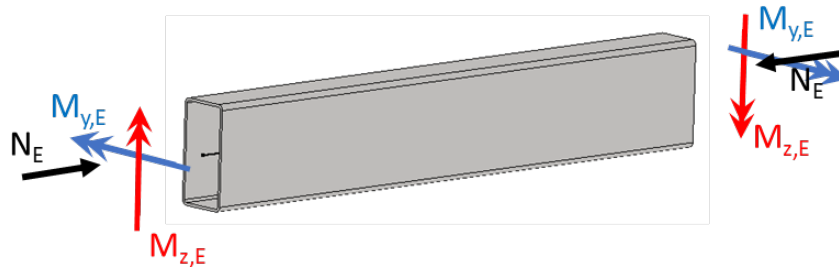


Figure 28: Schematic representation of the worked example with applied load

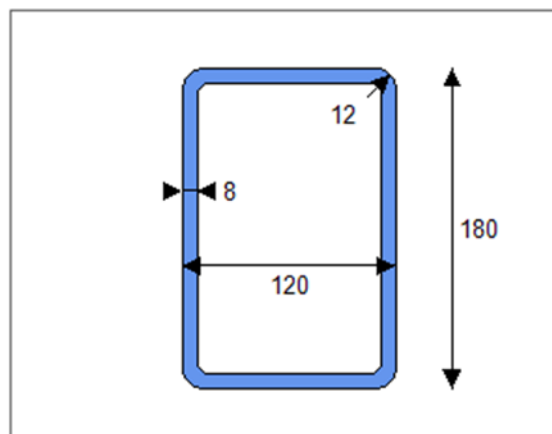


Figure 29: Cross-section dimensions

Cross-section properties

$$A = 44.75 \text{ cm}^2$$

$$I_y = 1950 \text{ cm}^4$$

$$W_{y,el} = 216.69 \text{ cm}^3$$

$$W_{y,pf} = 266.32 \text{ cm}^3$$

$$I_z = 1030 \text{ cm}^4$$

$$W_{z,el} = 171.3 \text{ cm}^3$$

$$W_{z,pf} = 200.2 \text{ cm}^3$$

Load

$$N_E = 1000 \text{ kN}$$

$$M_{y,E} = 60 \text{ kNm}$$

$$M_{z,E} = 13 \text{ kNm}$$

5.2.1 Design according to EC3

To determine the resistance according to the Eurocode, the cross-section needs to be classified first.

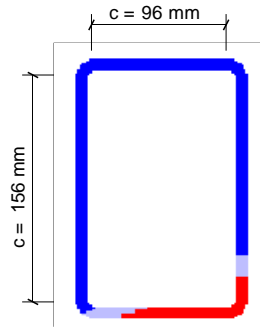


Figure 30: Plastic stress distribution, with c values for the purposes of classification

Figure 30 shows a plastic stress distribution under combined load. We can see the web of the section to be fully compressed, and so we classify it as such.

$$\varepsilon = \sqrt{\frac{235 \text{ MPa}}{f_y}} = 0.715$$

$$c_{\text{flange}} = b - 3t = 96 \text{ mm}$$

$$c_{\text{web}} = h - 3t = 156 \text{ mm}$$

$$\frac{c_{\text{flange}}}{t} = 12$$

$$\frac{c_{\text{web}}}{t} = 19.5 \leq 28\varepsilon = 20.01 \rightarrow \text{Class 1}$$

Both the flange and the web of the section satisfy the condition of Class 1, we will use clause 8.2.9.1 of prEN-1993-1-1 for the design. This is an iterative procedure, using an amplification factor R_{EC3} , to reach a value of 1.0 in (8.56) (prEN1993-1-1:2018).

$$M_{N,yRd} = M_{pl,y,Rd} \frac{1 - nR_{EC3}}{1 - 0.5\alpha_w} = 71.14 \text{ kNm}$$

$$M_{N,zRd} = M_{pl,z,Rd} \frac{1 - nR_{EC3}}{1 - 0.5\alpha_t} = 48.82 \text{ kNm}$$

WORKED EXAMPLES

$$\alpha_f = \frac{(A - 2ht)}{A} = 0.356 \quad \text{but} \quad \alpha_f \leq 0.5$$

$$\alpha_w = \frac{(A - 2bt)}{A} = 0.571 \quad \text{but} \quad \alpha_w \leq 0.5$$

$$\alpha_w = 0.5$$

$$\left(\frac{R_{EC3} M_{y,Ed}}{M_{N,y,Rd}} \right)^{\alpha_y} + \left(\frac{R_{EC3} M_{z,Ed}}{M_{N,z,Rd}} \right)^{\alpha_z} = 1.0$$

with:

$$\alpha_y = \alpha_z = \frac{1.66}{1 - 1.13n^2} ; n = \frac{R_{EC3} N_E}{N_{pl,R}} = 0.56$$

$$R_{EC3} = 1.162$$

$$\left(\frac{R_{EC3} M_{y,Ed}}{M_{N,y,Rd}} \right)^{\alpha_y} + \left(\frac{R_{EC3} M_{z,Ed}}{M_{N,z,Rd}} \right)^{\alpha_z} = 0.997$$

According to EC3, we can multiply the acting load by a factor of 1.162 to reach the plastic resistance limit of the cross-section.

5.2.2 *HOLLOSSTAB* design method

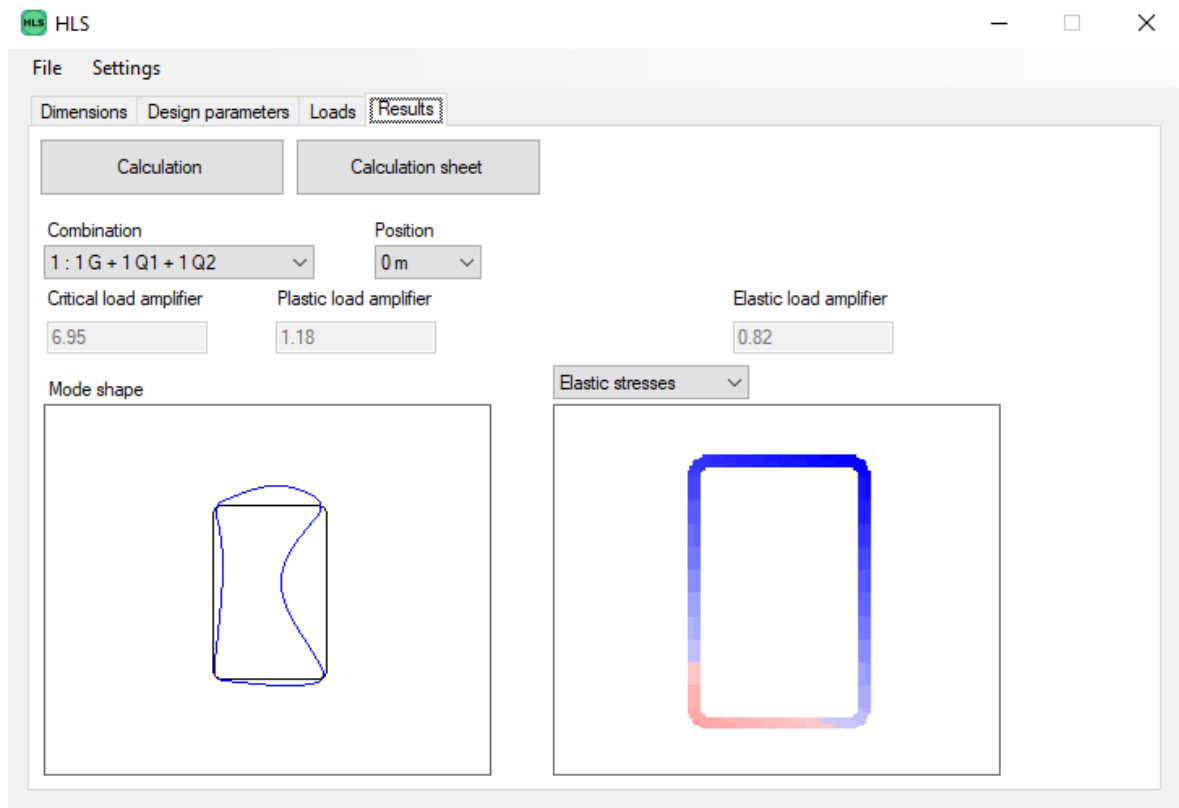


Figure 31: “Results” window of the HLS software

$$R_{el} = 0.82$$

$$R_{cr} = 6.95$$

$$\bar{\lambda}_L = \sqrt{R_{el}/R_{cr}} = 0.343$$

$$R_{pl} = 1.18$$

It is necessary to calculate the elastic stresses distribution in the cross-section under combined load, to find the highest and the second highest value of ψ .

$$\psi_1 = \text{MAX} \left(\frac{\frac{N}{A} + \frac{M}{W_y} - \frac{M}{W_z}}{\frac{N}{A} + \frac{M}{W_y} + \frac{M}{W_z}} ; \frac{\frac{N}{A} - \frac{M}{W_y} + \frac{M}{W_z}}{\frac{N}{A} + \frac{M}{W_y} + \frac{M}{W_z}} \right)$$

$$\psi_2 = \text{MIN} \left(\frac{\frac{N}{A} + \frac{M}{W_y} - \frac{M}{W_z}}{\frac{N}{A} + \frac{M}{W_y} + \frac{M}{W_z}} ; \frac{\frac{N}{A} - \frac{M}{W_y} + \frac{M}{W_z}}{\frac{N}{A} + \frac{M}{W_y} + \frac{M}{W_z}} \right)$$

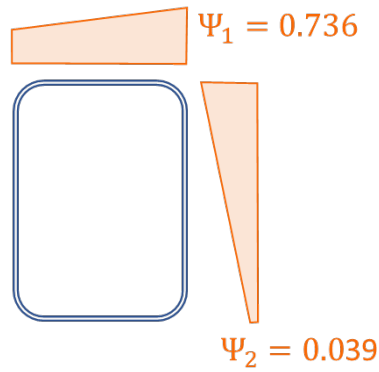


Figure 32: Graphical representation of the ψ values

$$B_2 = 1 ; A = (0.2 + 0.02\psi_2) \frac{(1+\psi_1)}{2} = 0.174 ; \bar{\lambda}_0 = 0.5 + \sqrt{0.25 - A} = 0.775$$

for $\bar{\lambda}_L \leq \bar{\lambda}_0$:

$$\chi_L = 1 + (\alpha_{pl} - 1) \cdot \frac{\bar{\lambda}_0 - \bar{\lambda}_L}{\bar{\lambda}_0 - 0,3} \leq \alpha_{pl}$$

with:

$$\alpha_{pl} = \frac{R_{pl}}{R_{el}} \leq 1,5 ; \alpha_{pl} = \frac{R_{pl}}{R_{el}} = \frac{1.18}{0.82} = 1.439 \leq 1.5$$

$$\chi_L = 1 + (1.439 - 1) \cdot \frac{0.775 - 0.343}{0.775 - 0,3} = 1.399 \leq \alpha_{pl}$$

$$R_{L,HS} = R_{el} \cdot \chi_L = 0.82 \cdot 1.399 = 1.148$$

The resulting value is the amplification factor for the applied load $R_{L,HS} = 1.148$.

5.2.3 Summary of results

$$R_{EC3} = 1.162$$

$$R_{L,HS} = 1.148$$

$$R_{GMNIA} = 1.16$$

$$U_{EC3} = \frac{1}{R_{EC3}} = 0.86$$

$$U_{L,HS} = \frac{1}{R_{L,HS}} = 0.871$$

$$U_{GMNIA} = \frac{1}{R_{GMNIA}} = 0.86$$

$$\frac{R_{L,HS}}{R_{EC3}} = 0.99$$

In this example, the utilizations of the two design methods are nearly identical the one predicted by GMNIA.

5.3 Example 3 - Cross-Sectional Capacity, RHS 200x100x6.3, EN10219, S460

Cross-section properties

$$A = 34.85 \text{ cm}^2$$

$$I_y = 1740 \text{ cm}^4$$

$$W_{y,el} = 173.9 \text{ cm}^3$$

$$W_{y,pf} = 219.1 \text{ cm}^3$$

$$I_z = 591 \text{ cm}^4$$

$$W_{z,el} = 118.2 \text{ cm}^3$$

$$W_{z,pf} = 135.4 \text{ cm}^3$$

Load

$$N_{Ed} = 640 \text{ kN}$$

$$M_{y,Ed} = 70.0 \text{ kNm}$$

$$M_{z,Ed} = 6.8 \text{ kNm}$$

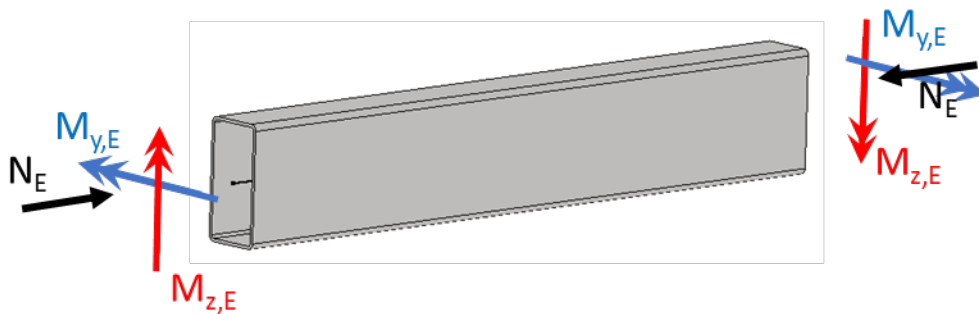


Figure 33: Schematic representation of the worked example with applied loads

5.3.1 Design according to EC3

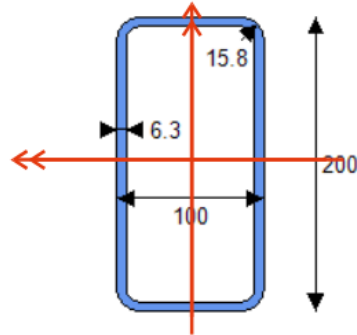


Figure 34: Cross-section dimensions

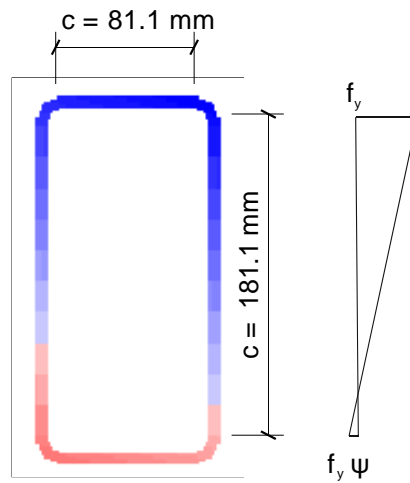


Figure 35: Elastic stress distribution, with c values for the purposes of classification

$$\varepsilon = \sqrt{\frac{235 \text{ MPa}}{f_y}} = 0.715$$

$$c_{\text{flange}} = b - 3t = 81.1 \text{ mm}$$

$$c_{\text{web}} = h - 3t = 181.1 \text{ mm}$$

$$\frac{c_{\text{flange}}}{t} = 12.9$$

$$\psi = -0.25 ; \alpha_c = \frac{(181 - 9)}{181} = 0.95$$

$$\frac{188\varepsilon}{6.53\alpha - 1} = 25.8 < \frac{c_{\text{web}}}{t} = 28.7 \leq \frac{38\varepsilon}{0.608 + 0.343\psi + 0.049\psi^2} = 51.7 \rightarrow \text{class 3}$$

$$W_{ep,y} = W_{pl,y} - (W_{pl,y} - W_{el,y})\beta_{ep,y} = 219 \text{ cm}^3 ; W_{ep,z} = W_{pl,z} - (W_{pl,z} - W_{el,z})\beta_{ep,z} = 118 \text{ cm}^3$$

$$\beta_{ep,y} = \max\left(\frac{\frac{C_{flange}}{t} - 34\varepsilon}{4\varepsilon}; 0\right) = 0$$

$$\beta_{ep,z} = \max\left(\frac{\frac{C_{web}}{t} - 34\varepsilon}{4\varepsilon}; 0\right) \leq 1, 0 = 1$$

$$M_{ep,y,Rd} = \frac{W_{ep,y} f_y}{\gamma_{M0}} = 100.80 \text{ kNm}$$

$$M_{ep,z,Rd} = \frac{W_{ep,z} f_y}{\gamma_{M0}} = 54.39 \text{ kNm}$$

$$n = \frac{R_{EC3} \cdot N_{Ed}}{N_{pl,Rd}} = 0.36$$

$$M_{N,ep,y,Rd} = M_{ep,y,Rd} (1 - n) = 64.42 \text{ kNm}$$

$$M_{N,ep,z,Rd} = M_{ep,z,Rd} (1 - n) = 34.76 \text{ kNm}$$

$$\left(\frac{R_{EC3} \cdot M_{y,Ed}}{M_{N,ep,y,Rd}}\right)^{\alpha_y} + \left(\frac{R_{EC3} \cdot M_{z,Ed}}{M_{N,ep,z,Rd}}\right)^{\alpha_z} = 1.0$$

$$\alpha_y = \alpha_z = \frac{1.66}{1 - 1.13n^2}; \quad R_{EC3} = 0.904$$

5.3.2 *HOLLOSSTAB* design method

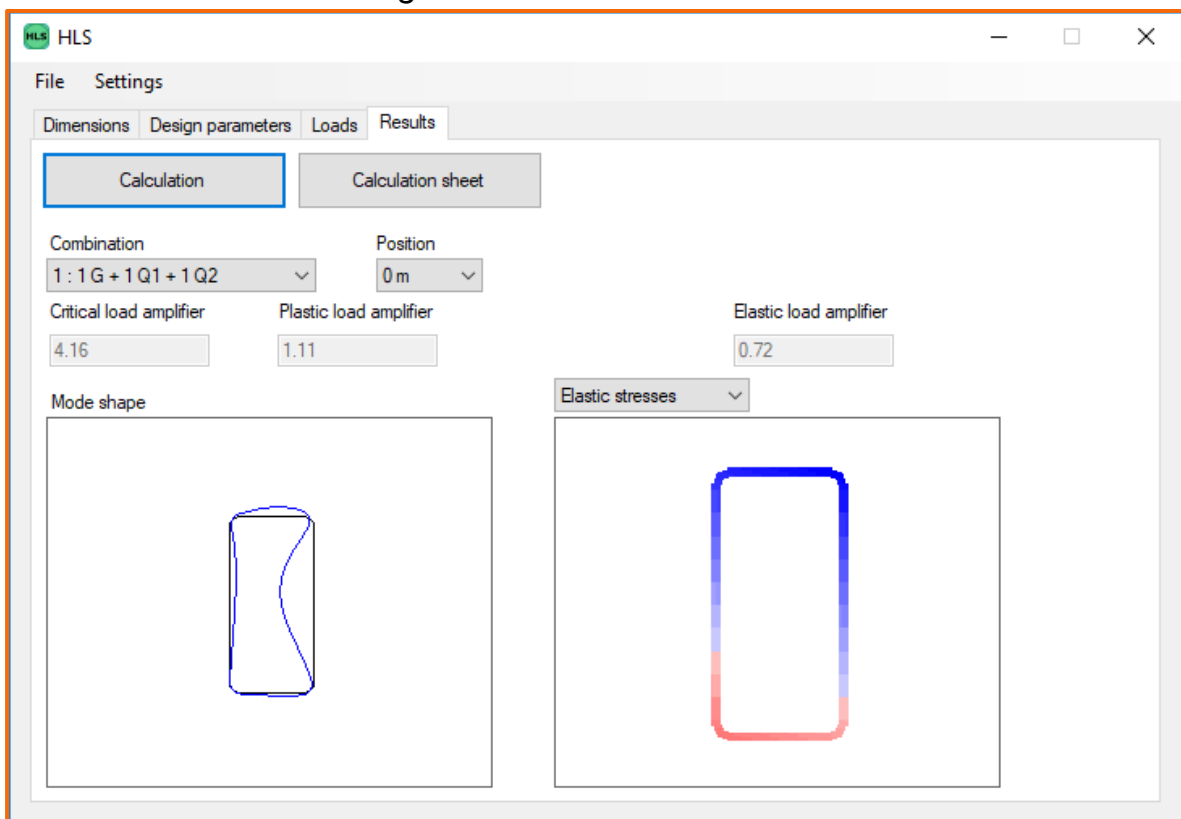


Figure 36: “Results” window of the *HLS* software

$$R_{el} = 0.72$$

$$R_{cr} = 4.16$$

$$\rightarrow \bar{\lambda}_L = \sqrt{R_{el}/R_{cr}} = 0.416$$

$$R_{pl} = 1.11$$

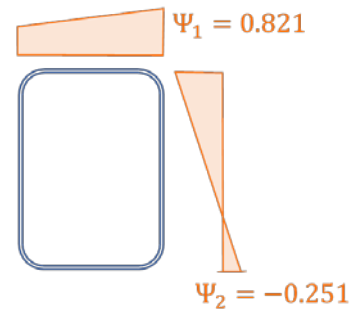


Figure 37: Graphical representation of the ψ values

$$\bar{\lambda}_L = 0.416$$

$$B_2 = 1$$

$$A = (0.225 + 0.025\psi_2) \frac{(1 + \psi_1)}{2} = 0.199$$

$$\bar{\lambda}_0 = 0.5 + \sqrt{0.25 - A} = 0.726$$

$$\text{for } \bar{\lambda}_L \leq \bar{\lambda}_0$$

$$\chi_L = 1 + (\alpha_{pl} - 1) \cdot \frac{\bar{\lambda}_0 - \bar{\lambda}_L}{\bar{\lambda}_0 - 0,3} \leq \alpha_{pl}$$

with:

$$\alpha_{pl} = \frac{R_{pl}}{R_{el}} \leq 1,5; \quad \alpha_{pl} = \frac{R_{pl}}{R_{el}} = \frac{1.06}{0.72} = 1.542 \geq 1.5 \rightarrow \alpha_{pl} = 1.5$$

$$\chi_L = 1 + (1.4 - 1) \cdot \frac{0.725 - 0.416}{0.725 - 0,3} = 1.364 \leq \alpha_{pl}$$

$$R_{L,HS} = R_{el} \cdot \chi_L = 0.72 \cdot 1.364 = 0.982$$

$$U_{L,HS} = \frac{1}{R_{L,HS}} = 1.019$$

5.3.3 Summary of results

$$R_{EC3} = 0.904$$

$$R_{L,HS} = 0.982$$

$$R_{GMNIA} = 1.130$$

$$U_{EC3} = \frac{1}{R_{EC3}} = 1.106$$

$$U_{L,HS} = \frac{1}{R_{L,HS}} = 1.019$$

$$U_{GMNIA} = \frac{1}{R_{GMNIA}} = 0.885$$

$$\frac{R_{L,HS}}{R_{EC3}} = 1.086$$

The results show that the cross-sectional resistance prediction of the new GSRM method is 8,6% higher than the current Eurocode design methodology for the studied section, while still being around 13% on the safe side compared to the realistic GMNIA resistance.

5.4 Example 4 - Cross-Sectional Capacity, EHS200x100x10, EN10210-2, S355

Cross-section properties

$$A = 45.69 \text{ cm}^2$$

$$I_y = 1716.20 \text{ cm}^4$$

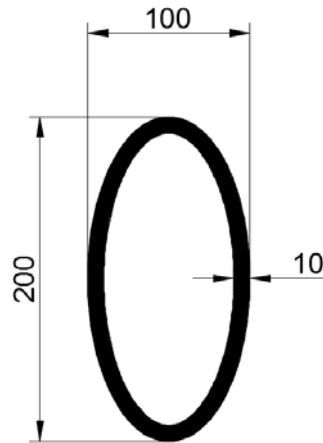
$$W_{y,el} = 171.62 \text{ cm}^3$$

$$W_{y,pf} = 245.73 \text{ cm}^3$$

$$I_z = 545.37 \text{ cm}^4$$

$$W_{z,el} = 109.07 \text{ cm}^3$$

$$W_{z,pf} = 146.27 \text{ cm}^3$$



Load

$$N_E = 235.7 \text{ kN}$$

$$M_{y,E} = 52.8 \text{ kNm}$$

$$M_{z,E} = 36.2 \text{ kNm}$$

Material properties:

Hot-rolled S355, $f_y = 355 \text{ N/mm}^2$, $f_u = 490 \text{ N/mm}^2$

5.4.1 Design according to EC3

Cross-section classification:

$$d_{e,c} \text{ for compression: } d_{e,c} = h^2/b = 400 \text{ mm}$$

$$d_{e,b} \text{ for major axis bending: } d_{e,b} = 0.4h^2/b = 160 \text{ mm}$$

$$\text{Modified axial force: } N_{mod,Ed} = N_{Ed} + M_{z,Ed}A/W_{pl,z} = 1364.5 \text{ kN}$$

$$\alpha_c = 0.88 \text{ (from numerical tool)}$$

$$d_e = d_{e,b} + (d_{e,c} - d_{e,b}) * (\alpha_c - 0.5) * 2 = 342.4 \text{ mm}$$

$$d_e/t \leq 70 - \text{Class 2}$$

Circular and elliptical hollow sections			
	Section in compression	Section in bending	Compression and bending
Class 1	$d_e/t \leq 50 \varepsilon^2$	$d_e/t \leq 50 \varepsilon^2$	$d_e/t \leq 50 \varepsilon^2$
Class 2	$d_e/t \leq 70 \varepsilon^2$	$d_e/t \leq 70 \varepsilon^2$	$d_e/t \leq 70 \varepsilon^2$
Class 3	$d_e/t \leq 90 \varepsilon^2$	$d_e/t \leq 140 \varepsilon^2$	$d_e/t \leq \frac{2520 \varepsilon^2}{5\psi + 23}$
Equivalent diameter d_e for circular and elliptical hollow sections			
For circular hollow sections:		$d_e = d$	
For elliptical hollow sections:			
In compression:		$d_e = h \left[1 + \left(1 - 2,3 \left(\frac{t}{h} \right)^{0,6} \right) \left(\frac{h}{b} - 1 \right) \right]$ or, conservatively: $d_e = \frac{h^2}{b}$	
In bending about the strong axis:		For $h/b \leq 1,36$: $d_e = \frac{b^2}{h}$	For $h/b > 1,36$: $d_e = 0,4 \frac{h^2}{b}$
In bending about the weak axis, or compression and bending about the weak axis:		$d_e = \frac{h^2}{b}$	
In compression and bending about the strong axis, the equivalent diameter d_e may be determined by linear interpolation between the equivalent diameter for compression and that for bending based on the parameter α for Class 1 and Class 2 cross-sections and ψ for Class 3 and Class 4 cross-sections.			
In compression and biaxial bending, the equivalent diameter d_e may be taken as the interpolated equivalent diameter for compression and bending about the strong axis, as described above, but with α_c and ψ determined using a modified axial force equal to $N_{Ed} + M_{z,Ed} A / W_{pl,z}$ for Class 1 and Class 2 cross-sections and $N_{Ed} + M_{z,Ed} A / W_{el,z}$ for Class 3 and Class 4 cross-sections.			

Figure 38: Design rules for cross-section classification of CHS and EHS in prEN 1993-1-1:2018

Plastic cross-section resistances under isolated loading:

$$\gamma_{M0} = 1$$

$$N_{pl,Rd} = Af_y / \gamma_{M0} = 1622.1 \text{ kN}$$

$$M_{pl,y,Rd} = W_{pl,y} f_y / \gamma_{M0} = 87.2 \text{ kNm}$$

$$M_{pl,z,Rd} = W_{pl,z} f_y / \gamma_{M0} = 51.9 \text{ kNm}$$

Cross-section interaction formulae:

$$n = N_{Ed} / N_{pl} = 0.145$$

$$M_{N,y,Rd} = M_{pl,y,Rd} (1 - n^{1.7}) = 84.0 \text{ kNm}$$

$$M_{N,z,Rd} = M_{pl,z,Rd} (1 - n^{1.7})^{1.18} = 49.6 \text{ kNm}$$

Cross-section check:

$$\alpha_y = 2, \alpha_z = 1.7$$

$$(M_{y,Ed} / M_{N,y,Rd})^2 + (M_{z,Ed} / M_{N,z,Rd})^{1.7} = 0.98 < 1 - \text{OK}$$

$$R_{EC3} = 1.01$$

For cross-sections where fastener holes may be neglected, the following approximation may be used for elliptical hollow sections of uniform thickness:

$$M_{N,y,Rd} = M_{pl,y,Rd}(1 - n^{1,7}) \quad (8.54)$$

$$M_{N,z,Rd} = M_{pl,z,Rd}(1 - n^{1,7})^{1,18} \quad (8.55)$$

(6) For bi-axial bending the following criterion should be satisfied:

$$\left(\frac{M_{y,Ed}}{M_{N,y,Rd}} \right)^{\alpha_y} + \left(\frac{M_{z,Ed}}{M_{N,z,Rd}} \right)^{\alpha_z} \leq 1 \quad (8.56)$$

— For elliptical hollow sections:

$$\alpha_y = 2; \alpha_z = 1,7$$

Figure 39: Cross-section design rules for EHS in prEN 1993-1-1:2018

5.4.2 HOLLOSSTAB design method (deformation-based approach)

R parameters (from numerical tool):

$$R_{el} = 0.73, R_{pl} = 1.04, R_{cr,L} = 20.91$$

$$\text{Local slenderness: } \bar{\lambda}_L = (R_{el} / R_{cr,L})^{1/2} = 0.187$$

Base curve:

$$\Psi = -0.85$$

$$\bar{\lambda}_0 = 0.43 - 0.07(1 + \Psi)^2/4 = 0.429$$

$$B_1 = 2.5 + (1 + \Psi)^2/4 = 2.506$$

$$\epsilon_{csm} / \epsilon_y = (\bar{\lambda}_0 / \bar{\lambda}_L)^{B_1} = 9.88$$

Material coefficients:

$$\epsilon_{sh} = 0.1 f_y / f_u - 0.055 = 0.017$$

$$\epsilon_{sh} / \epsilon_y = 10.32 > \epsilon_{csm} / \epsilon_y - \text{on the yield plateau}$$

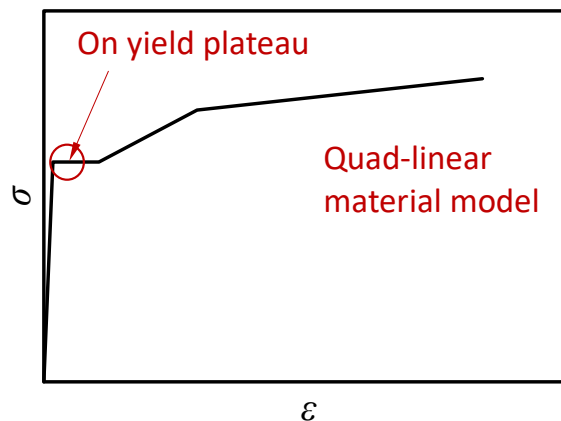


Figure 40: Quad-linear material model for hot-rolled sections

CSM-type resistance functions:

$$R_{b,L} = R_{csm} = R_{pl} \left(1 - \frac{(1 - R_{el}/R_{pl})}{(\epsilon_{csm}/\epsilon_y)^2} \right) = 1.04 > 1 - \text{OK}$$

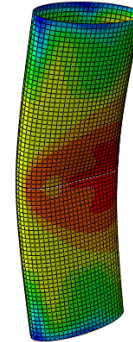
5.4.3 Summary of results

Assuming proportional loading:

$$R_{GMNIA} = 1.11$$

$$R_{EC3} = 1.01 - 9\% \text{ lower than } R_{GMNIA}$$

$$R_{b,L} = R_{csm} = 1.04 - 6\% \text{ lower than } R_{GMNIA}$$



The results show that the cross-sectional resistance prediction of the new CSM-GSRM method is 3% higher than the current Eurocode design methodology for the studied section, while still being around 6% on the safe side compared to the realistic GMNIA resistance.

5.5 Example 5 - Member Buckling, SHS200x200x6.3, EN10210, S690

Cross-section properties

$$A = 48.38 \text{ cm}^2$$

$$I_y = 3010 \text{ cm}^4$$

$$W_{y,el} = 301.04 \text{ cm}^3$$

$$W_{y,pf} = 350.25 \text{ cm}^3$$

$$I_z = I_y$$

$$W_{z,el} = W_{y,el}$$

$$W_{z,pf} = W_{y,pf}$$

Load

$$N_E = 1000 \text{ kN}$$

$$M_{y,E} = 100 \text{ kNm}$$

$$M_{z,E} = 25 \text{ kNm}$$

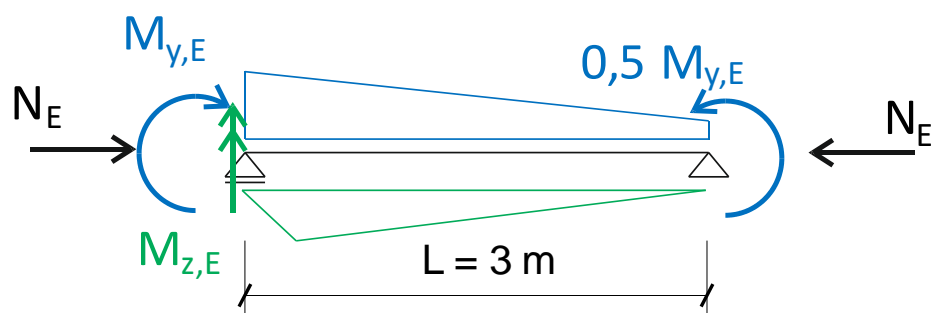


Figure 41: Schematic representation of the worked example with applied load

5.5.1 Design according to EC3

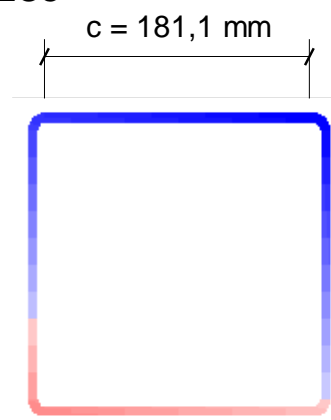


Figure 42: Dimensions and stress field to determine the cross-sectional properties

Effective cross section properties (EN1993-1-5)

Major axis bending $\rightarrow W_{y,eff}$

Flange in full compression

$$k_{\sigma} = 4.0 \quad , \quad \psi = 1.0$$

$$\bar{\lambda}_p = \frac{\frac{C_{flange}}{t}}{28.4 \varepsilon \sqrt{k_{\sigma}}} = 0.87$$

$$\rho = \frac{\bar{\lambda}_p - 0.055(3 + \psi)}{\bar{\lambda}_p^2} = 0.86$$

$$W_{y,eff} = 277 \text{ cm}^3$$

Minor axis bending $\rightarrow W_{z,eff}$

Web in full compression

$$k_{\sigma} = 4.0 \quad , \quad \psi = 1.0$$

$$\bar{\lambda}_p = \frac{\frac{C_{web}}{t}}{28.4 \varepsilon \sqrt{k_{\sigma}}} = 0.87$$

$$\rho = \frac{\bar{\lambda}_p - 0.055(3 + \psi)}{\bar{\lambda}_p^2} = 0.86$$

$$W_{z,eff} = 277 \text{ cm}^3$$

Compression $\rightarrow A_{eff}$

Flange

$$k_{\sigma} = 4.0 \quad , \quad \psi = 1.0$$

$$\bar{\lambda}_p = \frac{\frac{C_{flange}}{t}}{28.4 \varepsilon \sqrt{k_{\sigma}}} = 0.87$$

$$\rho = \frac{\bar{\lambda}_p - 0.055(3 + \psi)}{\bar{\lambda}_p^2} = 0.86$$

Web

$$k_{\sigma} = 4.0 \quad , \quad \psi = 1.0$$

$$\bar{\lambda}_p = \frac{\frac{C_{web}}{t}}{28.4 \varepsilon \sqrt{k_{\sigma}}} = 0.87$$

$$\rho = \frac{\bar{\lambda}_p - 0.055(3 + \psi)}{\bar{\lambda}_p^2} = 0.86$$

$$A_{eff} = 42.04 \text{ cm}^2$$

Load amplification factor (prEN1993-1-1)

$$\bar{\lambda}_y = \sqrt{\frac{N_{el}}{N_{cr,y}}} = 0.647$$

$$\bar{\lambda}_z = \sqrt{\frac{N_{el}}{N_{cr,z}}} = 0.647$$

$$\chi_y = \frac{1}{\Phi + \sqrt{\Phi^2 - \bar{\lambda}_y^2}} = 0.914$$

$$\chi_z = \frac{1}{\Phi + \sqrt{\Phi^2 - \bar{\lambda}_z^2}} = 0.914$$

$$n_y = \frac{REC3_G \cdot N_E}{\chi_y \cdot N_R} = 0.40$$

$$C_{my} = 0.8$$

$$k_{yy} = C_{my}(1 + 0.6\bar{\lambda}_y n_y) = 0.923$$

$$k_{zy} = 0.8k_{yy} = 0.739$$

$$n_z = \frac{REC3_G \cdot N_E}{\chi_z \cdot N_R} = 0.40$$

$$C_{mz} = 0.6$$

$$k_{zz} = C_{mz}(1 + 0.6\bar{\lambda}_z n_z) = 0.693$$

$$k_{yz} = k_{zz} = 0.693$$

Beam-column check

$$\frac{REC3_G \cdot N_E}{\chi_y \cdot N_R} + k_{yy} \frac{REC3_G \cdot M_{y,E}}{M_{y,R}} + k_{yz} \frac{REC3_G \cdot M_{z,E}}{M_{z,R}} = 1.0$$

$$\frac{REC3_G \cdot N_E}{\chi_z \cdot N_R} + k_{zy} \frac{REC3_G \cdot M_{y,E}}{M_{y,R}} + k_{zz} \frac{REC3_G \cdot M_{z,E}}{M_{z,R}} = 1.0$$

$$REC3_G = 1.053$$

Cross-section check

$$REC3_L = \frac{1}{\frac{N_E}{A_{eff} f_y} + \frac{M_{y,E}}{W_{y,eff} f_y} + \frac{M_{z,E}}{W_{z,eff} f_y}} = 1.001$$

$$REC3 = \min(REC3_G, REC3_L) = 1.001$$

5.5.2 *HOLLOSSTAB* design method

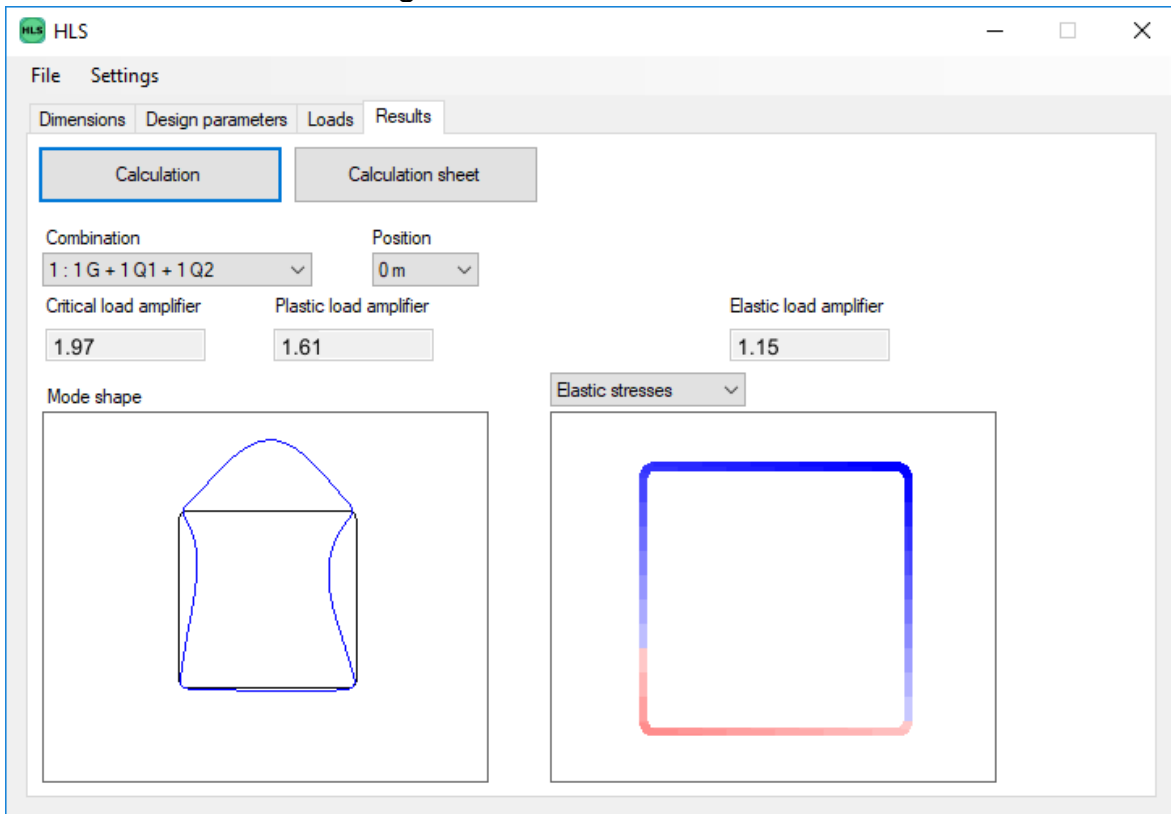


Figure 43: “Results” window of the HLS software

$$R_{el} = 1.15$$

$$R_{cr} = 1.97$$

$$\rightarrow \bar{\lambda}_L = \sqrt{R_{el} / R_{cr}} = 0.762$$

$$R_{pl} = 1.61$$

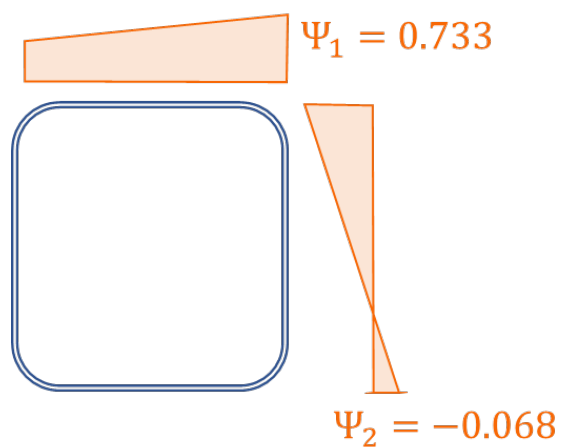


Figure 44: Graphical representation of the ψ values

$$R_{el} = 1.15 \quad R_{cr} = 1.97$$

$$\rightarrow \bar{\lambda}_L = \sqrt{R_{el}/R_{cr}} = 0.762$$

$$B_2 = 1$$

$$A = (0.2 + 0.02\psi_2) \frac{(1 + \psi_1)}{2} = 0.172$$

$$\bar{\lambda}_0 = 0.5 + \sqrt{0.25 - A} = 0.779$$

$$\text{for } \bar{\lambda}_L \leq \bar{\lambda}_0$$

$$\chi_L = 1 + (\alpha_{pl} - 1) \cdot \frac{\bar{\lambda}_0 - \bar{\lambda}_L}{\bar{\lambda}_0 - 0.3} \leq \alpha_{pl}$$

with:

$$\alpha_{pl} = \frac{R_{pl}}{R_{el}} \leq 1.5$$

$$\alpha_{pl} = \frac{R_{pl}}{R_{el}} = \frac{1.61}{1.13} = 1.410 \leq 1.5$$

$$\chi_L = 1 + (1.41 - 1) \cdot \frac{0.779 - 0.734}{0.779 - 0.3} = 1.014 \leq \alpha_{pl}$$

$$R_{L,HS} = R_{el} \cdot \chi_L = 1.15 \cdot 1.014 = 1.16$$

$$\eta_y = \frac{\frac{M_{y,E}}{M_{el,y}}}{\frac{N_E}{N_{el}}} = 1.607$$

$$\eta_z = \frac{\frac{M_{z,E}}{M_{el,z}}}{\frac{N_E}{N_{el}}} = 0.402$$

$$c_0 = 1 + \eta_y + \eta_z = 3.009$$

$$\chi_L = \frac{R_{el}}{R_L} = 1.014$$

$$R_{cr,y} = \frac{N_{cr,y}}{N_E} = 6.932$$

$$R_{cr,z} = \frac{N_{cr,z}}{N_E} = 6.932$$

$$\bar{\lambda}_{G,y} = \sqrt{\frac{R_L}{R_{cr,y}}} = 0.409$$

$$\bar{\lambda}_{G,z} = \sqrt{\frac{R_L}{R_{cr,z}}} = 0.409$$

for $\chi_L \geq 1.0$

$$\rho = 0.5$$

$$\xi_{LG,y} = 1.0 + (\chi_L - 1)\rho \cdot \sqrt{c_0} \bar{\lambda}_{G,y} C_{m,y} = 1.0041$$

$$\xi_{LG,z} = 1.0 + (\chi_L - 1)\rho \cdot \sqrt{c_0} \bar{\lambda}_{G,z} C_{m,z} = 1.0041$$

$$\beta_{LG,y} = \frac{\xi_{LG,y}}{c_0} = 0.334$$

$$\beta_{LG,z} = \frac{\xi_{LG,z}}{c_0} = 0.334$$

$$\alpha_{EC3} = 0.13$$

$$\eta_{EC3,y} = \alpha_{EC3}(\bar{\lambda}_{G,y}\sqrt{c_0} - 0.2) = 0.066$$

$$\eta_{EC3,z} = \alpha_{EC3}(\bar{\lambda}_{G,z}\sqrt{c_0} - 0.2) = 0.066$$

$$\Phi_{G,y} = \frac{1}{2} \left[\beta_{LG,y} (1 + \eta_z C_{m,z} + \eta_y C_{m,y} + \eta_{EC3,y}) + \bar{\lambda}_{G,y}^2 \right] = 0.547$$

$$\Phi_{G,z} = \frac{1}{2} \left[\beta_{LG,z} (1 + \eta_z C_{m,z} + \eta_y C_{m,y} + \eta_{EC3,y}) + \bar{\lambda}_{G,z}^2 \right] = 0.547$$

$$\chi_{G,y} = \frac{1}{\Phi_{G,y} + \sqrt{\Phi_{G,y}^2 - \beta_{LG,y} \bar{\lambda}_{G,y}^2}} = 0.961 \quad ; \quad \chi_{G,z} = \frac{1}{\Phi_{G,z} + \sqrt{\Phi_{G,z}^2 - \beta_{LG,z} \bar{\lambda}_{G,z}^2}} = 1.000$$

$$R_{b,G+L,y} = \chi_{G,y} \cdot R_L = 1.116 \quad ; \quad R_{b,G+L,z} = \chi_{G,z} \cdot R_L = 1.161$$

$$R_{G+L,HS} = \min(R_{b,G+L,y}, R_{b,G+L,z}) = 1.116$$

5.5.3 Summary of results

$$R_{EC3} = 1.001$$

$$R_{G+L,HS} = 1.116$$

$$R_{GMNIA} = 1.260$$

$$U_{EC3} = \frac{1}{R_{EC3}} = 0.999$$

$$U_{G+L,HS} = \frac{1}{R_{G+L,HS}} = 0.894$$

$$U_{GMNIA} = \frac{1}{R_{GMNIA}} = 0.794$$

$$\frac{R_{G+L,HS}}{R_{EC3}} = 1.115$$

The results show that the member buckling resistance prediction of the new GSRM method is 11.5% higher than the current Eurocode design methodology for the studied member, while still being around 12% on the safe side compared to the realistic GMNIA resistance.

5.6 Example 6 - Member buckling, CHS60.3x3, EN10219-2, S700

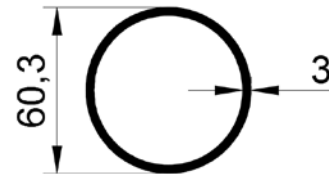
Cross-section properties

$$A = 5.40 \text{ cm}^2$$

$$I = 22.22 \text{ cm}^4$$

$$W_{el} = 7.37 \text{ cm}^3$$

$$W_{pF} = 9.86 \text{ cm}^3$$



Load

$$N_E = 126.4 \text{ kN}$$

$M_E = 1.73 \text{ kNm}$, uniform bending moment along the length

Material properties:

Cold-formed S700, $f_y = 700 \text{ N/mm}^2$, $f_u = 750 \text{ N/mm}^2$

Effective length: 1104 mm, pinned-pinned at both ends

5.6.1 Design according to EC3

Cross-section check: similar to Worked Example 5

Cross-section classification – Class 2

Cross-section check – OK

Member buckling check:

Relative slenderness $\bar{\lambda}$:

$$\bar{\lambda} = (Af_y / N_{cr})^{1/2} = 1.00$$

Column buckling resistance:

$\alpha = 0.49$ for cold-formed CHS

$$\phi = 0.5(1 + \alpha(\bar{\lambda} - 0.2) + \bar{\lambda}^2) = 1.20$$

$$\chi = 1/(\phi + (\phi^2 - \bar{\lambda}^2)) = 0.54$$

$$\gamma_{M0} = \gamma_{M1} = 1$$

$$N_{b,Rd} = \chi N_{c,Rd} = \chi Af_y = 204.1 \text{ kN}$$

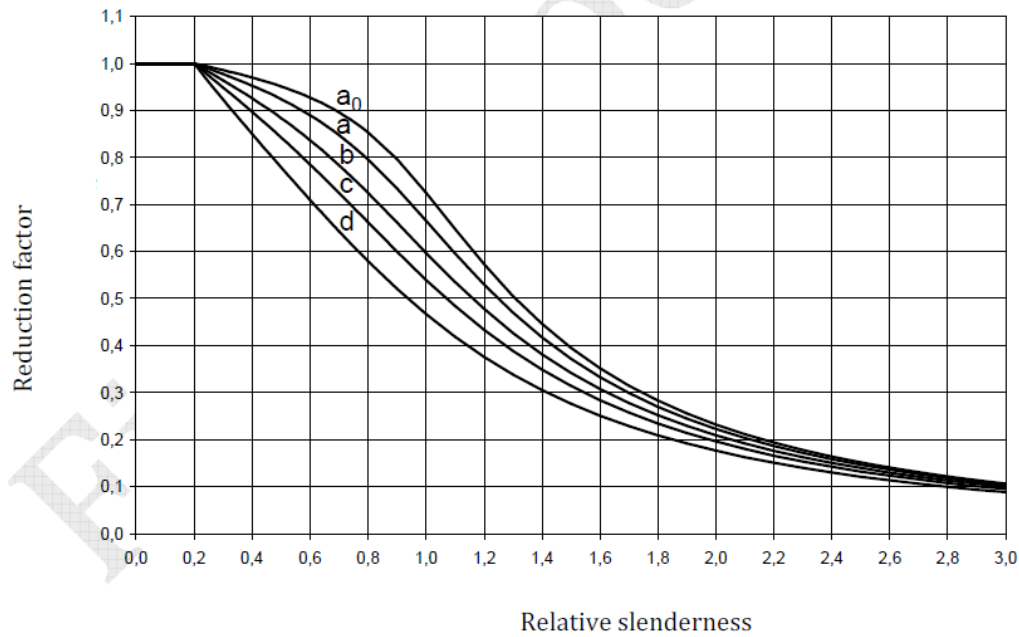


Figure 45: EC3 column buckling curves

Bending moment resistance:

$$M_{c,Rd} = M_{pl,Rd} = W_{pl}f_y = 6.90 \text{ kNm}$$

Beam-column interaction formulae:

$$C_m = 1 \text{ for uniform bending}$$

$$n = N_{Ed} / N_{b,Rd} = 0.62$$

$$k = C_m(1 + 0.8n) = 1.50$$

$$N_{Ed}/N_{b,Rd} + kM_{Ed}/M_{c,Rd} = 0.99 < 1$$

$$R_{EC3} = 1.0$$

Member buckling check – OK

(5) Members which are subjected to combined bending and axial compression should satisfy **Formula (8.85)** and **Formula (8.86)**:

$$\frac{N_{Ed}}{\chi_y N_{Rk}} + k_{yy} \frac{M_{y,Ed} + \Delta M_{y,Ed}}{\chi_{LT} \frac{M_{y,Rk}}{\gamma_{M1}}} + k_{yz} \frac{M_{z,Ed} + \Delta M_{z,Ed}}{\frac{M_{z,Rk}}{\gamma_{M1}}} \leq 1,0 \quad (8.85)$$

$$\frac{N_{Ed}}{\chi_z N_{Rk}} + k_{zy} \frac{M_{y,Ed} + \Delta M_{y,Ed}}{\chi_{LT} \frac{M_{y,Rk}}{\gamma_{M1}}} + k_{zz} \frac{M_{z,Ed} + \Delta M_{z,Ed}}{\frac{M_{z,Rk}}{\gamma_{M1}}} \leq 1,0 \quad (8.86)$$

Table 8.7 — Interaction factors k_{yy} and k_{yz} for Formula (8.85)
Instability governed by buckling about y-y axis

Plastic cross-sectional properties Class 1, Class 2, Class 3 (with W_{ep} according to Annex B)	Elastic cross-sectional properties Class 3 (with W_{el}), Class 4
For $\bar{\lambda}_y < 1,0$: $k_{yy} = C_{my} [1 + (\bar{\lambda}_y - 0,2) n_y]$	For $\bar{\lambda}_y < 1,0$: $k_{yy} = C_{my} (1 + 0,6 \bar{\lambda}_y n_y)$
For $\bar{\lambda}_y \geq 1,0$: $k_{yy} = C_{my} (1 + 0,8 n_y)$	For $\bar{\lambda}_y \geq 1,0$: $k_{yy} = C_{my} (1 + 0,6 n_y)$
$k_{yz} = 0,6 k_{zz}$, See Table 8.8	$k_{yz} = k_{zz}$, See Table 8.8
NOTE 1 See (9) for n_y .	
NOTE 2 See (10) and Table 8.9 for C_{my}	

Figure 46: Design rules for beam-columns in prEN 1993-1-1:2018

5.6.2 HOLL0SSTAB design method

R parameters (from numerical tool):

$$R_{el} = 1.53, R_{pl} = 1.99, R_{cr,L} = 29.96, R_{cr,G} = 2.99$$

Cross-section check: similar to Worked Example 5

$$R_{b,L} = 2.04 > 1 - \text{OK}$$

Global buckling check:

$$\text{Global slenderness: } \bar{\lambda}_G = (R_{b,L} / R_{cr,G})^{1/2} = 0.83$$

Local-global modification factor:

$$k = (R_{cr,G} / R_{b,L})^{1/4} = 1.10$$

$$\beta_{LG} = (1 - (1 - R_{el} / R_{b,L}) / k) = 0.78$$

Imperfection factor:

$$\Psi = (N_{Ed}/A - M_{Ed}/W_{el}) / (N_{Ed}/A + M_{Ed}/W_{el}) = 0$$

$$\alpha = 0.3(1-\Psi) + 0.6\varepsilon = 0.65$$

Global buckling resistance:

$$\eta = \alpha(\beta_{LG}^{1/2} \bar{\lambda}_G - 0.2) = 0.34$$

$$\phi = 0.5(1 + \eta + \beta_{LG} \bar{\lambda}_G^2) = 0.93$$

$$\chi_G = \beta_{LG} / (\phi + (\phi^2 - \beta_{LG} \bar{\lambda}_G^2)^{1/2}) = 0.51$$

$$R_{b,L+G} = \chi_G R_{b,L} = 1.04 > 1 - \text{OK}$$

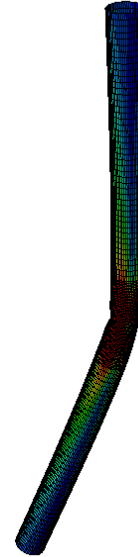
5.6.3 Summary of results

Assuming proportional loading:

$$R_{GMNIA} = 1.11$$

$$R_{EC3} = 1.00 - 10\% \text{ lower than } R_{GMNIA}$$

$$R_{b,L+G} = 1.04 - 7\% \text{ lower than } R_{GMNIA}$$



The results show that the member buckling resistance prediction of the new GSRM method is 4% higher than the current Eurocode design methodology for the studied member, while still being around 7% on the safe side compared to the realistic GMNIA resistance.

REFERENCES

- [1] Eurocode 3: Design of steel structures – Part 1-1: General rules and rules for buildings, CEN - European Committee for Standardization, Brussels, version EN 1993-1-1, 2005.
- [2] Eurocode 3: Design of steel structures – Part 1-1: General rules and rules for buildings, CEN - European Committee for Standardization, Brussels, Draft standard under review by National Standardisation Bodies, version prEN 1993-1-1, 2018.
- [3] Szalai, J.; Papp F.: Theory and Application of the General Method of Eurocode 3 Part 1-1, Proc. of EUROSTEEL 2011, Budapest, Hungary, August 31 - September 2, 2011.
- [4] Tankova, T.; Marques, L.; Andrade, A.; Simões da Silva, L.: A consistent methodology for the out-of-plane buckling resistance of prismatic steel beam-columns, *Journal of Constructional Steel Research*, 128, pp. 839-853, London/Amsterdam: Elsevier, 2017.
- [5] Schafer, B.W.: Review: The Direct Strength Method of cold-formed steel member design, *Journal of Constructional Steel Research*, 64, Issue 7-8, pp. 766-778, London/Amsterdam: Elsevier, 2008.
- [6] Schafer, B. W.: Advances in the direct strength method of thin-walled steel design, Eighth International Conference on Thin-Walled Structures (ICTWS), 2018.
- [7] Taras, A.: Derivation of DSM-type resistance functions for in-plane global buckling of steel beam-columns, *Journal of Constructional Steel Research*, 105, pp. 95-113, London/Amsterdam: Elsevier, 2016.
- [8] Gardner, L.: The Continuous Strength Method. *Proceedings of the Institution of Civil Engineers - Structures and Buildings*. 161(3), 127-133, London/Amsterdam: Elsevier, 2008.
- [9] Yun, X.; Gardner, L.: The continuous strength method for the design of cold-formed steel non-slender tubular cross-sections, *Engineering Structures*, 175, pp.549-564, Elsevier, November 2018.
- [10] Boissonnade, N.; Hayeck, M.; Saloumy, E.; Nseir, J.: An Overall Interaction Concept for an alternative approach to steel members design, *Journal of Constructional Steel Research*, 135, pp.199-212, London/Amsterdam: Elsevier, 2017.
- [11] Toffolon, A.; Taras, A.: Development of an OIC-Type local buckling design approach for cold-formed unstiffened and groove-stiffened hollow sections, *Thin-Walled Structures*, 144, June, 2019.
- [12] Greiner, R.; Kettler, M.; Lechner, A.; Freytag, B.; Linder, J.; Jaspart, J.-P.; Boissonnade, N.; Bortolotti, E.; Weynand, K.; Ziller, C.; Oerder, R.: Final Report: SEMI-COMP: Plastic Member Capacity of Semi-Compact Steel Sections - a more Economic Design, Research Fund for Coal and Steel Project SEMI-COMP, Grant Nr. RFSR-CT-2004-00044, 2008.
- [13] Taras, A.; Toffolon, A.; Niko, I.; Gardner, L.; Meng, X.; Silvestre, N.: Cross-sectional resistance / local buckling of RHS & SHS, *HOLLOSSTAB*, RFCS Grant Nr. 2015-709892, Deliverable 4.2, Munich, 2019.
- [14] Gardner, L.; Meng, X.; Taras, A.; Toffolon, A.: Cross-sectional resistance / local buckling of CHS & EHS, *HOLLOSSTAB*, RFCS Grant Nr. 2015-709892, Deliverable 3.2, London, 2019.
- [15] Toffolon, A.; Müller, A.; Niko, I.; Taras, A.: Experimental and numerical analysis of the local and interactive buckling behaviour of hollow sections, *Proceedings of SDSS 2019*, Prague, 2019.
- [16] Taras, A.; Toffolon, A.; Gardner, L.; Meng, X.: Background on the development of Overall-Slenderness based design rules for RHS and SHS, *HOLLOSSTAB*, RFCS Grant Nr. 2015-709892, Deliverable 8.2, Munich, 2019.

WORKED EXAMPLES

- [17] Gardner, L.; Meng, X.; Taras, A.; Toffolon, A.: Background on the development of Overall-Slenderness based design rules for CHS and EHS, *HOLLOSSTAB*, RFCS Grant Nr. 2015-709892, Deliverable 8.3, London, 2019.
- [18] Beyer, A.; Bureau, A.; Taras, A.; Toffolon, A.: Reliability Analysis of the Design Proposals and Determination of Partial Factors, *HOLLOSSTAB*, RFCS Grant Nr. 2015-709892, Deliverable 7.2, Paris, 2019.
- [19] Vieira, L.; Martins, A.; Gonçalves, R.; Camotim, D.; Silvestre, N.; Beyer, A.; Bureau, A.: Software Tools, *HOLLOSSTAB*, RFCS Grant Nr. 2015-709892, Deliverable 8.4, Lisbon, 2019.
- [20] EN 10219: Cold formed welded structural hollow sections of non-alloy and fine grain steels, CEN – European Committee for Standardization, Brussels, 2006.
- [21] EN 10210: Hot finished structural hollow sections of non-alloy and fine grain steels, CEN – European Committee for Standardization, Brussels, 2006.
- [22] Winter, G.: Strength of thin steel plates compression flanges, *Transactions of the American Society of Mechanical Engineers*, 112(1), pp. 527-554, 1946
- [23] Eurocode 3: Design of steel structures - Part 1-5: General rules - Plated structural elements, CEN - European Committee for Standardization, Brussels, version EN 1993-1-5, 2006.
- [24] Schillo, N.; Taras, A.; Feldmann, M.: Assessing the reliability of local buckling of plates for mild and high strength steels, *Journal of Constructional Steel Research*, 142, pp. 86-98, London/Amsterdam: Elsevier, 2018.
- [25] Simões da Silva, L.; Tankova, T.; Marques, L.; Rebelo, C.; Kuhlmann, U.; Kleiner, A.; Snijder, H.H.; Dekker, R.W.A.; Dehan, V.; Taras, A.; Haremza, C.; Cajot, L.-G.; Vassart, O.; Popa, N.: Standardization of Safety Assessment Procedures across Brittle to Ductile Failure Modes – Final Report - SAFEBRITILE, Research Fund for Coal and Steel, Grant Nr. RFSR-CT-2013-00044, 2017.
- [26] Simões da Silva, L.; Tankova, T.; Marques, L.; Rebelo, C.; Taras, A.: Safety assessment of Eurocode 3 stability design rules for the lateral-torsional buckling of prismatic beams, *Advanced Steel Construction*, 14, Issue 4, pp. 668-693, Hong-Kong, 2018.